Research Square

Preprints are preliminary reports that have not undergone peer review.
They should not be considered conclusive, used to inform clinical practice,
or referenced by the media as validated information.

Ground Motion Parameters For the 2015 Nepal Earthquake

Jahnabi Basu (jahnabi.basu18@gmail.com)
Indian Institute of Technology Madras
Bhargavi Podili
Indian Institute of Technology Madras
S. T. G. Raghukanth
Indian Institute of Technology Madras
D Srinagesh
NGRI: National Geophysical Research Institute CSIR

Research Article

Keywords: Ground Motion Parameters, Rupture distance, Sediment depth, Instantaneous Frequency and Ground Motion Prediction Equation

Posted Date: October 15th, 2021

DOI: https://doi.org/10.21203/rs.3.rs-797752/v1

License: This work is licensed under a Creative Commons Attribution 4.0 International License.
Read Full License

Ground motion parameters for the 2015 Nepal Earthquake

Jahnabi Basu*[a], Bhargavi Podili[a], S. T. G. Raghukanth[a] and D Srinagesh[b]

[a]Department of Civil Engineering, Indian Institute of Technology Madras, Chennai, India
[b]CSIR - National Geophysical Research Institute, Uppal Road, Hyderabad, Telangana 500007, India

*For correspondence
Email: jahnabi.basu18@gmail.com
Phone: +91-7085338505

Declarations

Funding
The authors did not receive support from any organisation for the submitted work.

Conflicts of interests/Competing interests
The authors have no conflicts of interest to disclose that are relevant to the content of this article.

Availability of data and material
Strong-motion data of the Gorkha earthquake sequence from the Central Indo-Gangetic Network (CIGN) are obtained collaboratively from D. S. Srinagesh at srinagesh@ngri.res.in. The ground motion records for stations KTP, PTN, TVU, and THM were made available by CESMD (Center for Engineering Strong Motion Data) (Takai et al. 2016), whereas station KATNP was made available by USGS (USGS, 2015b).

Code availability
Custom codes in MATLAB are used in the current study.

Authors' contributions
Formal analysis, investigation and writing-original draft preparation: Jahnabi Basu, Writing-review and editing and Supervision: Bhargavi Podili, Conceptualization, Methodology and Supervision: S. T. G. Raghukanth, Data provision: D Srinagesh. All authors read and approved the final manuscript.

Ethics approval

Compliance with Ethical Standards
No Human Participants and/or Animals are involved in the research.

Consent to participate
Not applicable

Consent to publication
Not applicable

ABSTRACT

The 25th April 2015 Nepal earthquake is the first major event in the Himalayan orogeny that provides a relatively well recorded dataset. This paper presents a comprehensive analysis of the mainshock and its five major aftershocks through 21 well established ground motion parameters. The analysis is presented for near field stations of the Kathmandu basin and far field stations of the Indo-Ganga basin, including the site response behavior with varying sediment thickness. In addition, a new ground motion model is derived for all the 21 parameters using moment magnitude, rupture distance, site class and sediment depth as predictor variables.

Keywords: Ground Motion Parameters; Rupture distance; Sediment depth; Instantaneous Frequency and Ground Motion Prediction Equation

1. INTRODUCTION

The Himalayan tectonic zone of the Indian subcontinent has been constantly subjected to incessant seismic activities, wherein a total of eight major earthquakes of M_w>7 are recorded in the past two centuries. These include the 1866 Nepal (M_w 7.4), 1897 Shillong (M_w 8.1), the 1905 Kangra (M_w 7.8), the 1934 Bihar-Nepal (M_w 8.1), the 1947 Arunachal Pradesh (M_w 7.9), the 1950 Arunachal Pradesh (M_w 8.6), the 2005 Muzafferapur (M_w 7.6) and the 2015 Nepal (M_w 7.9) earthquakes. The most common and unfortunate aspect among all these events is that none of these earthquakes are recorded, until the M_w 7.9 Nepal earthquake, thus a thorough study of this 2015 event gained extreme importance. The 25th April 2015 Nepal earthquake originated near the Main Frontal Thrust of the Himalayas, which is at the subduction plate boundary between the Indian and Eurasian plates. The rupture originated in the Gorkha district (28.147°N and 84.708°E), which is nearly 80 km to the northwest of the capital city – Kathmandu and propagated eastwards for about 160 km. Ground failure was reported in many densely populated areas, where the main event triggered landslides and ground liquefaction in the areas surrounding Kathmandu. There was unprecedented damage to buildings and heritage structures, where the economic loss is nearly 10 billion USD, which is about half the GDP of Nepal and the human loss includes over 9000 fatalities. Several moderate to strong aftershocks followed this main event. According to USGS, 227 earthquakes of M_w> 4.1 were recorded within 250km radius of the main event epicentre and in three weeks prior and after the main event. Among these, there are 30 aftershocks of M_w> 5 and five aftershocks of M_w>6 due to the M_w 7.9 rupture. In order to perform a thorough study of the region, the five major aftershocks are also included in the analysis.

In the immediate aftermath, many studies were conducted on source rupture characteristics (Hayes *et al.*, 2015, Galetzka *et al.*, 2015, Grandin *et al.*, 2015) and on artificial simulation of ground motions (Koketsu *et al.,* 2016, Dhanya *et al.,* 2017). Some of the important observations drawn from these studies were the significant influence of rupture directivity and basin effects on ground motions. Among the few studies on ground motion datasets,

Goda *et al.* (2015) attributed the main cause of structural damage and collapse of buildings to the short period peak, which is due to ground vibration induced by near source rupture. Dhakal *et al.* (2016) confirmed that the basin sediments at the KATNP station amplified the long period components of ground motions and have concluded that the GMPEs of the similar tectonic environment such as Japan underestimate the recorded peak and spectral acceleration values. The ground motion study conducted by Takai *et al.* (2016) with the five time histories (KATNP, PTN, THM, KTP and TVU) in the Kathmandu valley has also emphasized the amplification due to valley response of sedimentary sites. These studies therefore emphasize the effect of the sedimentary basin response in the Kathmandu valley. The ground motions of the Nepal earthquake and its aftershocks were also recorded by the Central Indo-Gangetic Plains Network (CIGN) and the Indian Institute of Technology, Roorkee (IITR) networks of the Indo-Gangetic Plain (IGP). Due to the presence of substantial alluvial deposits, significant site amplifications in the IGP sites were noticed previously (Srinagesh *et al.*, 2011; Singh *et al.*, 2020). Therefore, it would be interesting to study the site response of both the Kathmandu valley and the IGP. Chadha *et al.* (2016) and Rajaure *et al.* (2016) have obtained site amplifications for some of the IGP and Kathmandu stations for the Nepal earthquake, using a Fourier based approach. However, an advanced non-stationary approach including the evolutionary characteristics of the ground motion would yield better results. Moreover, higher order parameters such as the Root-Mean-Square acceleration (a_{RMS}), Cumulative absolute velocity (CAV), Arias Intensity (I_a) etc., and spectral parameters extracted from Fourier spectrum, Power spectral density and evolutionary power spectral density functions would extract important information from the ground motions, that was not explored previously. Therefore, in the present study, the ground motions of the Nepal earthquake and its aftershocks are studied using a total of 21ground motion parameters (GMPs) representing various amplitude, frequency and duration characteristics of the ground motion.

Many local and regional ground motion models are available for the Himalayan region of India (Sharma *et al.*, 2009, Nath *et al.,* 2005, 2012, Raghukanth and Iyengar, 2006, 2007, Joshi *et al.*, 2013 etc.). Among these models, very few ground motion prediction equations (GMPEs) are derived using strong motion datasets (Sharma *et al.*, 2009, Bajaj and Anbazhagan, 2019) and the ground motion datasets that have been used to derive many of these GMPEs via regression analysis, does not include ground motions of an earthquake of magnitude M_w 7.9. Moreover, among the few available GMPEs that are derived by including the Nepal earthquake data (Singh *et al*., 2017), most were obtained for standard GMPs such as PGA, PGV and Spectral accelerations. There are few global models available for higher order parameters such as CAV and I_a (Campbell and Bozorgnia, 2010, Foulser-Piggot and Goda, 2014). However, since these models are derived for a different tectonic environment, the applicability as well as the goodness of these models to the Indian scenario is debatable. Hence, there is a necessity to generate a new set of GMPEs using the Nepal mainshock and aftershock datasets, especially for the higher order parameters. Therefore, this paper presents a thorough analysis of the 2015 Nepal earthquake and its aftershocks through 21 well established GMPs. The behavior of these GMPs with distance from the source, distance, sediment depth and site characteristics is also studied. Since it is observed that the GMPEs

available for the Nepal region are unable to capture the exact trend in the data for the M_w 7.9 earthquake, a ground motion prediction model is also developed for all the GMPs and the attenuation relations are validated through residual analysis and through comparison with the local as well as global GMPEs that are applicable to the region. In addition, the hierarchy of the current model against the entire local as well as the global models is validated through a ranking system.

2. STRONG MOTION DATABASE

2.1. Strong Motion Data

Despite being seismically active, a nationwide seismic monitoring network is not available in Nepal. However, four datasets of records are obtained here from four different sources: The United States Geological survey (USGS), Hokkaido University, Japan and Tribhuvan University, Nepal (HU-TU), Central Indo-Gangetic Plains Network (CIGN) and the Indian Institute of Technology, Roorkee (IITR). As discussed in the literature, the first set of ground motion records were provided by USGS at the KATNP (Kantipath, Kathmandu) station (USGS, 2015b). Along with the main event, this station has recorded accelerograms of seven aftershocks. Later, the collaborated effort of Hokkaido University, Japan and Tribhuvan University, Nepal (HU-TU) provided four strong motion records for the 2015 main shock at stations KTP, PTN, THM and TVU. Both these sets of acceleration time histories were made available through CESMD (Center for Engineering Strong Motion Data) (Takai *et al.* 2016). The relatively new CIGN network comprise of 26 strong motion stations, 19 of which are located in the IGP (Chadha *et al.*, 2016); whereas the IITR seismic network of around 100 accelerographs in the IGP (Kumar *et al.* 2012). However, due to technical issues, the main shock of the 2015 earthquake was recorded by just 15 CIGN stations and 13 IITR stations. The number of recording stations is even lower for the succeeding aftershocks. Based on the records available, ground motions of the M_w 7.9 2015 Nepal earthquake and its accompanying five major aftershocks are considered in the present study. Table 1 gives the details of these aftershocks, which range between M_w 5.3 - M_w7.2 and were dated just within a month of the main event. Fig. 1 shows the epicentres of all the earthquakes considered in the current study, along with the distribution of the ground motion recording stations.

2.2. Seismo-tectonics and site geology of the region

The Himalayan front is divided into four major tectonic divisions from south to north, which were demarcated by the presence of physiographic transition zones in the form of prominent faults (Gansser, 1964; Validya, 1964). The four tectonic divisions include – Sub Himalaya, Lesser Himalaya, High Himalaya and Tethyan Himalaya. The southernmost division i.e., the Sub Himalaya is separated from the IG plain by the Himalayan Frontal Thrust (HFT), which is sometimes also referred to as the Main Frontal Thrust (MFT). Other prominent faults from south to north include Main Boundary Thrust (MBT), Main Central Thrust (MCT), and the South Tibetan Detachment System (STDS). Nepal is diversified with all the four tectonic divisions, wherein the Kathmandu valley is located in the Lesser Himalayan belt (Sakai *et al.*, 2002). It can be observed from the seismo-tectonic map given in Fig. 1 that the earthquake

rupture originated in the MCT and the effect of these tremors was felt even in the IGP whereas the impact of these tremors was severe in the Kathmandu valley. It is to be noted here that each of the tectonic divisions is characterised with similar physiography and the thickness of sedimentary deposits usually decreases from north to south. Therefore, sediment depth is considered as an important attribute to the ground motions considered in this study and thus, the sediment depth of each ground motion recording station is obtained from 1D velocity models given by Bijukchhen *et al.* (2017) and Dhakal *et al.* (2016). In addition, the average velocity in the top 30 metres of the soil strata (V_s30) is regarded as the representative of site characteristics. The V_s30 values for the IGP sites are obtained from the SPT-N studies of Anbazhagan and Bajaj (2020) and theV_s30 values for the sites in the Kathmandu basin are obtained from Bijuckhhen et al. (2017) and USGS. Table 2 gives NEHRP Site classification based on the V_s30, as given by IBC, 2009. The details of all the 40 ground motion recording stations along with the respective sediment depth and NEHRP site class are given in Table 3.

2.3. Preliminary Studies

In the present study, 155 ground motions recorded at 40 stations due to a total of six earthquakes are used for the analysis. Since it is established that the current study include analysis of ground motions in the IGP as well, the range of distance measure is considered from 10 to 1000 km. Fig. 2 shows the distribution of strong motion records used in the present study with respect to moment magnitude (M_w) and rupture distance (R_{rup}). It can be observed that the dataset consist of near field records with R_{rup} as low as 12 km and far field records with R_{rup} as high as 896 km. Histograms showing the number of records with respect to M_w, R_{rup} and hypocentral depth are given in Fig. 3.

The raw data recorded by CIGN and IITR stations with a sampling rate of 100 Hz is subjected to a baseline correction of 0.1 to 25 Hz. On the other hand, HU-TU data with a sampling rate of 200 Hz is corrected from 0.1 to 49.5 Hz. Overall, the highest PGA of the dataset is observed to be 0.265g at the near-field station KTP. Interestingly, the observed PGA values are unexpectedly lower for such an earthquake which is notorious for severe structural damage. Fi. 4 shows the acceleration time histories (EW, NS and UD component) of the main event for stations KTP, THM and AMT. It is observed that among the two near-field stations KTP and THM, the PGA recorded is slightly higher for KTP due to lower R_{rup} than that of THM (0.14g). In comparison to these stations, the station AMT which is located in the IGP is observed to have significantly lower PGA value (0.017g). Spectral acceleration plots of the respective ground motion time histories are obtained in Fig. 5, to observe any underlying pattern with respect to the period. Predominant long period amplitudes are observed clearly for Kathmandu basin stations – TVU, PTN and THM, wherein all of these are located on sediment sites. On the other hand, low period predominant amplitude is observed in the case of the station KTP, which is located on rock hard strata. Hence, sediment depth is considered as an important factor to which ground motion amplifications of the current dataset can be attributed. However, such long period amplifications at sediment sites in the IG basin are not clearly identified from the spectral acceleration plot. Therefore, detailed analysis of these ground motions are conducted via ground motion parameters.

3. GROUND MOTION PARAMETERS

Ground motion parameters are essential for describing unique characteristics of the ground motions in a short, compact and quantitative form. Thus, parameters representing peak values such as PGA, PGV and PGD are more prevalent among engineers for seismic design and linear structural analysis. But, peak values solely are not sufficient to characterize damage potential completely. Therefore, many other GMPs like Vertical-to-Horizontal (V/H) spectral ratio, Root-Mean-Square acceleration (a_{RMS}), Arias Intensity (I_a), etc. were developed and were correlated with structural damage. Bhargavi and Raghukanth (2018, 2019) have presented a total of 21 such parameters and have rated the damage potential of a ground motion using principal component analysis. The same 21 parameters are selected to analyze the ground motions considered in the current study. Amplitude, frequency content and duration are the three significant characteristics of a ground motion (Kramer, 1996)**.** Thus, based on the dependence of a parameter on the number of these essential ground motion characteristics, GMPs are broadly categorized into three classes: First order, second order and third order parameters. The basic definitions of all the ground motion parameters obtained from the acceleration time histories are explained in table 4.

3.1. First Order Parameters

First order parameters which represent only one key characteristic include Peak Ground Acceleration (PGA), Peak Ground Velocity (PGV), and Peak Ground Displacement (PGD). Combinations of these parameters like V/H ratio of PGA and PGA/PGV ratio are also shown as better characterisations of ground motions. Seismic damage is complicated and difficult to interpret solely on the basis of peak values of the ground motion. Therefore parameters such as PGA, PGV and PGD are insufficient to determine the damage potential of an earthquake. Thus, frequency content based parameters are estimated through analysis of the time history in the frequency domain using Fourier Amplitude Spectra (FAS) and Power Spectra. Venmarke (1976) proposed central frequency and shape factor as the indicators of statistical properties of Power Spectral Density (PSD) function, using spectral moments. Predominant frequency is measured as the frequency corresponding to maximum value of the Fourier amplitude spectrum. Similarly, a duration parameter – Significant duration, which depends on the ground motion time history, is considered. Significant duration is defined as the time interval between 5% and 95% energy thresholds of the of Husid plot (Husid, 1969).

Extremely low values of the entire peak GMPs including PGV and PGD, are recorded for all the IG basin records, compared to that of the Kathmandu basin records. The predominant frequencies of records at near field sediment sites are of the order 0.2, whereas the predominant frequency obtained at the station KTP is of the order 3.4. Once again, these values clearly indicate the presence of predominant low frequency i.e., long period amplitudes in the ground motions recorded at sediment sites of the Kathmandu basin. On the other hand, even though predominant frequencies as high as 3 and 7.5 are recorded at some sites in the IG basin, no clear pattern is observed with the variation of these values with the sediment depth. Interestingly, the central frequencies (Ω) of vertical component of ground motion records are greater (double in most cases) to that of the horizontal component, for

both the Kathmandu and IG basins. However, the $V/H_{(PGA)}$ values are less than 1 for most of these cases. Further, the parameter 'q', which represents bandwidth of the time history, is almost same in both the components (Horizontal and Vertical), if not slightly higher for horizontal component of the ground motions. Therefore, based on the definition of 'Ω' and 'q', it can be assumed that the horizontal component of these ground motions have registered almost the same amount of energy at lower frequencies to that of the vertical component concentrated at high frequencies. As expected, significant durations of near field records of the Kathmandu basin are extremely low to that of the far field IG basin records. All the primary parameters for two near field stations – 'KTP' and 'THM' in the Kathmandu basin and one far field station – 'AMT' in the IGP basin are tabulated in table 5.

3.2. Second Order Parameters

First order parameters are not sufficient for complete characterisation of the ground motion. Housner and Jennings(1964) proposed Root-Mean-Square acceleration (a_{RMS}) as an indicator of damage as it considers the acceleration time history over significant duration of Husid plot. Arias intensity was introduced to observe the cumulative effects of ground motion over the complete Duration. Benioff (1934) proposed Response Spectra as a quantification of the physical response of structures due to ground shaking. Housner (1952) derived spectrum intensities from the pseudo velocity response spectrum to measure the intensity of ground shaking between periods of 0.1s to 2.5s. Park *et al.* (1985) introduced a new secondary parameter as the characteristic intensity in terms of a_{RMS} and significant duration, which is linearly related to damage index due to maximum deformation and absorbed hysteretic energy (Ang *et al.*, 1990). Acceleration Spectral Intensity (ASI) was developed by VonThun *et al.* (1988) to characterize ground motion at higher frequencies. Electrical Power Research Institute (EPRI**,** 1988) mathematically defined a ground motion intensity measure named cumulative absolute velocity (CAV) as an efficient indicator of structural damage. Reed and Kassawara (1990) proposed CAV for determining the exceedance of the Operating Basis Earthquake (OBE) after the occurrence of an earthquake at a nuclear power plant.

In the preliminary analysis it was noted that maximum PGA of 0.265g was observed at the station KTP, despite KTP being on a rock site. It should be noted that all the four stations of the HU-TU network including the KTP station are located at almost similar rupture distances. Therefore, this preliminary result would be considered an inconsistency from the common notion that soft soil sites or sediment sites usually register larger ground motion amplitudes. Upon the analysis of the second order parameters, it was revealed that the sediment sites indeed recorded larger amplitudes. The highest a_{RMS} value of the dataset – 0.055g is obtained for the station TVU, whereas the a_{RMS} value for the highest recorded PGA component of KTP is 0.036g. In fact, all the other second order amplitude parameters such as I_a, CAV and I_c are higher for the record of station TVU over the record at KTP. This is due to the reason that the significant duration of the former ground motion is greater than the latter. Results like these emphasize the importance of second order parameters over first order parameters such as PGA, PGV and PGD. Table 5 shows the secondary parameters i.e., a_{RMS}, I_a, CAV, I_c, ASI, VSI etc. for stations KTP, THM and AMT.

3.3. Third Order Parameters

An acceleration time history is highly stochastic and non-stationary. Thus, the statistical properties vary in both temporal and spectral domain simultaneously. Therefore, parameters reflecting non-stationarity of ground motions became popular. The concept of evolutionary power spectral density was introduced by Priestley (1965), which gives an account of the temporal and frequency evolution of time history. To address non-stationarity in ground motion, Liu (1970b) used instantaneous power spectrum models. However, PSD does not exist for non-stationary processes. Huang *et al.* (1998) proposed that nonlinear and non-stationary data can be handled through Empirical Mode Decomposition (EMD) with Hilbert-Huang transformation (HHT). Wu and Huang (2009) modified the EMD as an Ensemble EMD, which includes the shifting of an ensemble of white noise modulated signals to remove signal intermittency. Raghukanth and Sangeetha (2012) have presented the detailed procedure for obtaining EPSD for ground motions using EMD-HHT method. In the present study, Ensemble Empirical Mode Decomposition (EEMD) is used to obtain EPSD where the acceleration time history is decomposed into simple empirical oscillatory modes called Intrinsic Mode Functions (IMFs). An IMF is defined as a time series where the number of extrema and the number of zero crossings must either be equal or differ by one. Further, the mean value of the envelopes defined by the local maxima and minima of the IMF is zero. Thus obtained IMFs are orthogonal to each other. Initially, a white noise of negligible amplitude is added to the acceleration time history. From the resulting signal, the consecutive maxima and minima are identified. These maxima and minima are connected as cubic splines to obtain the upper and lower envelopes. Thus IMFs are obtained by removing local median in every step through a shifting procedure. This process is continued until a monotonic function is obtained at the end. Once the IMFs are obtained, the Hilbert Transform of these IMFs is used to construct EPSD. An Analytic Function (AF_j) is formed from the conjugate pair of obtained IMF (IMF_j) and Hilbert Transform of the respective IMF ($hIMF_j$) to calculate the corresponding amplitude (C_j) and instantaneous frequency (ω_j) of EPSD. The amplitude of energy in time is combined over different frequencies for the extracted IMFs to obtain the energy distribution in the time-frequency domain in the form of a surface plot of EPSD ($\mathrm{G}(\omega, \mathrm{t})$).

$$AF_j = IMF_j(t) + ihIMF_j(t) = C_j(t)e^{-i\omega(t)} \tag{1}$$

$$C_j(t) = \sqrt{\left[IMF_j^2(t) + hIMF_j^2(t)\right]} \tag{2}$$

$$\omega_j(\mathrm{t}) = \frac{\mathrm{d}}{\mathrm{dt}}\left[\tan^{-1}\left(\frac{hIFM_j(t)}{IMF_j(t)}\right)\right] \tag{3}$$

$$\mathrm{G}(\omega, \mathrm{t}) = \sum_{\mathrm{i}=1}^{\mathrm{n}} \frac{1}{2}[C_j(IMF_i)]^2 \tag{4}$$

The EPSD plots thus obtained for the near field stations in Kathmandu valley (KTP, PTN, THM and TVU) as well as the far field IGP stations (VNS, AMT, BSR and TDR) and their respective time histories are shown in Figure 6. The energy distribution varying with time and frequency can be visualized here and it can be observed that energy distribution in these evolutionary spectra is concentrated over the frequency of 6-8 Hz for the near field stations.

The EPSD function is considered as the third order GMP and its statistical properties are characterised using: Total Energy (E_{acc}) of the EPSD, first and second moments of the frequency and time axes: Spectral Centroid (E_w), Spectral standard deviation (S_w) and Temporal Centroid (E_t), Temporal standard deviation (S_t) and, the Correlation coefficient of the time and frequency. All the 21 GMPs derived for the three stations – KTP, THM and AMT are shown in Table 5.

3.3.1 Analysis using IMFs and instantaneous frequencies

The IMFs of the acceleration time history (EW) for four stations in the IG basin: VNS, AMT, BSR and TDR and four stations in the Kathmandu basin: KTP, TVU, PTN and THM, along with their respective percentage variances are shown in Figure 7. The original signal can be expressed as the sum of these IMFs. The percentage of variance of each IMF is defined as the contribution of each IMF to the total variance of the data. In majority of cases in the present study, the original data can be reconstructed using the first 10 IMFs. It can be observed that for VNS station, the first four IMFs are sufficient to recreate 93% of the ground motion where the first IMF represents 52% of the original data. For the station AMT, first five IMFs are required to regenerate 94% of the original time history with both first and second IMF having percentage variance of 25%. For station BSR, 95% of the ground motion can be obtained by adding up the first six IMFs. In this case, the second IMF is more dominant than the first IMF, with 24% of the total variance. For station TDR, IMF4 is predominant with 19% of the variance of ground motion, and the first six IMFs are required to reproduce 93% of the ground motion. Thus, it can be assumed that as the thickness of sediments in the IG basin increases from south to north, the IMFs with higher modes becomes predominant.

In case of the station KTP, which is located at a hard rock site of the Kathmandu basin, first five IMFs are essential for rebuilding the original ground motion. Here, the maximum percentage variance is observed for the first IMF, representing 38% of the original data. For stations PTN, THM, TVU and KATNP located at sediment sites, higher IMFs (third to sixth IMF) are more dominant. For instance, IMF3 constitute 30% of the variance for station TVU. On the other hand, IMF4 represents 49% of the ground motion for station THM and 30% of the ground motion for station PTN. Moreover, IMF6 constitute 54% of the variance for station KATNP. Therefore, it is inferred that IMFs with higher modes are indeed predominant for ground motions recorded on sediment sites of the Kathmandu valley as well.
The estimated instantaneous frequencies from IMFs of acceleration time histories for both IG basin and Kathmandu basin are shown in Figure 8. Table 6 shows the mean and standard deviation of the instantaneous frequency, along with the percentage variances of the first 10 IMFs for all the ground motion records of the Mw 7.9 earthquake. According to the definition of IMFs, the mean instantaneous frequency of the IMFs decreases in the higher modes. Moreover, the instantaneous frequency corresponding to the dominant IMF i.e., the IMF with maximum percentage of variance, is considered as the dominant frequency of the acceleration time history. Consequently, it is observed that the dominant frequencies of the IG basin stations -VNS, AMT, BSR and TDR are 7.2 Hz, 9.6 Hz, 5 Hz and 1.3 Hz respectively. Therefore, the dominant mean instantaneous frequencies are decreasing as the R_{rup} increases and the thickness of the sediment increases. In order to observe this property, the dominant

IMFs and their corresponding mean instantaneous frequencies are plotted against sediment depth in Figure 9. Even though there is no underlying pattern in the dominant IMFs of the data at intermediate rupture distances, it can be observed that the higher modes are prevalent for larger sediment depths at larger distances as well as at near field distances. Further, a decent trend can be observed in Figure 9(b), wherein the dominant mean instantaneous frequencies are decreasing with the sediment depth, especially for the CIGN records. Srinagesh *et al.* (2011) conducted analysis of the IG basin and provided the fundamental frequencies of the basin, wherein these fundamental frequencies increases (from 0.13 to 0.8) with a decrease in the sediment thickness (from north to south of the basin). Consequently, significant amplifications due to sediment depth are expected at the site's fundamental frequency. Therefore, it is assumed that significant amplifications due to the sediment depth are not observed in many of the far field ground motions that were recorded in the IG basin. However, in order to obtain amplifications at each of these sites, a HHT based procedure is adopted.

3.3.2 HHT based site amplification

In this section, site amplification analysis is carried out to provide a greater understanding of the effect of sediment depth on ground motions over short and long time periods. Several techniques have been in use to perform the site response analysis, of which the most common procedure involves comparing the Horizontal-to-Vertical Spectral Ratio (HVSR). However, this method is infamous for not estimating the exact amplification value and therefore limits its application. Various other methods based on Fourier spectral analysis such as the Standard spectral ratio (SSR) technique and the Ratio of source spectrum (RSS) technique were suitable for the present scenario and they have been successfully used previously to estimate the site amplification in the IGP and Kathmandu basins (Chadha *et al*., 2016; Singh *et al*., 2020; Rajaure *et al*., 2016). However, the studies considering Fourier-based amplification assumes linear behavior of the sites sediments. In Fourier-based estimation, frequency is constant for the entire length of data window where as HHT-based frequency content analysis considers temporal non-stationarity as well. Therefore, the effect of site nonlinearity on the ground motion time histories can be characterized by estimating site amplification based on the marginal spectrum obtained from the HHT (Zhang, 2006). It is defined as the ratio of marginal Hilbert amplitude spectra of sedimentary sites to hard rock sites, which is similar to the SSR technique involving Fourier based analysis. The marginal Hilbert amplitude spectra $A(\omega)$ over a temporal duration T of the ground motion and the HHT based amplification factor ($FH_s(\omega)$) are given in equations 5 and 6 respectively.

$$A(\omega) = \int_0^T G(\omega, t)dt \tag{5}$$

$$FH_s(\omega) = \frac{\sqrt{A_{s,EW}^2 + A_{s,NS}^2}}{\sqrt{A_{r,EW}^2 + A_{r,NS}^2}} \tag{6}$$

Here, $G(\omega, t)$ is the EPSD; the subscripts EW and NS represent two horizontal components and subscripts s and r represent the target sedimentary site and reference hard rock site respectively. The HHT-based amplifications thus obtained at sedimentary sites of IGP and Kathmandu basin for M_w 7.9 mainshock are shown in figure 10. Site amplification factors are estimated for VNS, AMT, BSR and TDR stations in the IG basin considering hard reference sites as ALB, ALM, ALM and RPG respectively. Similarly, the KTP station is considered as a reference hard rock site for TVU, PTN, THM and KATNP in the Kathmandu basin. In order to compare these values with the Fourier based amplifications, the corresponding plots are obtained for the IGP and KB sites using the procedure given Chadha *et al*. (2016) and Rajaure *et al*. (2016) respectively. It can be observed from the figure that HHT-based dominant frequency is similar to the fundamental frequency obtained using Fourier based method for most of the sites in IGP. A slight diminution can be observed at the HHT- based dominant frequency at some stations in Kathmandu basin. However, a significant increase in the amplification values can be observed at these frequencies for HHT- based method than the Fourier based method.

The amplifications obtained for the four far field stations VNS, AMT, BSR and TDR of the IG basin for the M_w 7.9 mainshock and the two aftershocks of M_w 6.7 and M_w 5.3 are shown in figure 11. It can be observed that the HHT- based dominant frequency is same for M_w 7.9 mainshock and M_w 5.3 aftershock for IGP stations. The amplitude for the fifth aftershock (M_w 5.3) is much lesser than the M_w 7.9 mainshock and its immediate aftershock (M_w 6.7) for most of the stations in IGP. This is a fair observation since aftershocks are usually created along a ruptured fault, and hence have lower amplitude than mainshock. The increased site amplification at lower frequencies for the higher magnitude events can be considered as an indication of soil nonlinearity at these sites. Moreover, it should be noted that the sediment depth of the station VNS is much less compared to the other three sites. Therefore, the amplifications noticed at this site are not quite high as that of the other sites. At the same time, the amplifications for aftershocks noticed at this site are higher than mainshock. Thus, comparing with the other sites the station VNS shows weak or no site nonlinearity under the mainshock. However, the dataset used in the present study is considerably small and sparse to obtain a relation between sediment depth and site amplification. In fact, the amplification factors cannot be found for many sites in the IGP due to lack of information regarding a sufficiently close hard rock site. Moreover, the aftershock records at the near-field stations are not available for the Kathmandu basin. Therefore, given a comprehensive dataset, the nonlinear behavior and the effect of sediment depth on amplification of the site can be studied more comprehensively for insightful observations. Overall, the HHT based method proved to be a better option for obtaining site amplification.

4. GROUND MOTION MODEL

In this section, a region specific ground motion prediction equation (GMPE) is developed. A suitable GMPE is most important for predicting the future seismic potential of the region.

Due to lack of a comprehensive dataset, developing a regional GMPE for Himalayan orogeny is quite challenging. Despite of this, Singh *et al.* (2017) have developed empirical equations for the Himalayan region for three amplitude parameters: PGA, PGV and PGD. However, it will be interesting to develop new prediction equations for the traditional parameters as well as for those important for engineering applications like a_{RMS}, I_a, CAV etc. Due to small and sparse dataset, nonlinear mixed effect model (Abrahamson and Youngs, 1992) is used to develop GMPEs in the present study to incorporate both fixed and random effects. The algorithm for estimation of model parameters and variances involve estimating the parameters first using the fixed effects regression method. The most general framework of GMPE model is

$$\ln y_{ij} = f\left(M_i, R_{ij}, \theta\right) + \eta_i + \epsilon_{ij} \tag{7}$$

Where Y_{ij} is a ground motion parameter, $\mu_{ij} = f\left(M_i, R_{ij}, \theta\right)$ is the attenuation equation, M is the measure of earthquake source, R is distance measure, θ is the vector of model parameters, η_i represents inter-event residual for event i and ϵ_{ij} represents intra-event residual for jth recording of event i.

4.1. Ground motion prediction equation

The predictor variables considered for the GMPE include M_w, R_{rup}, flags for Vs30 of the site (F_{Vs30}) and sediment depth variation (F_{sed}). In order to formulate attenuation relationships between a GMP and the predictor variables, the following simple functional form is selected for all the 21 GMPS:

$$\ln(GMP) = \ln(gmp) + \eta_i + \epsilon_{ij} \tag{8}$$

$$\ln(gmp) = f_{mag} + f_{dis} + f_{site} + f_{sed} \tag{9}$$

$$f_{mag} = c_0 + c_1 M \tag{10}$$

$$f_{dis} = c_2 R + c_3 \ln(R + c_4 exp(c_5 M)) \tag{11}$$

$$f_{site} = c_6 F_{Vs30} \tag{12}$$

$$f_{sed} = c_7 F_{sed} \tag{13}$$

$$\tau^2 = var(\eta_i) \text{ and } \sigma^2 = var(\epsilon_{ij}) \tag{14}$$

Here, f_{mag} represents the magnitude term where coefficient c_0 corresponds to magnitude or absolute scale of the GMP (equation 8). The term $'c_1 M'$ represents effect on the ground motion concerning earthquake magnitude considered as source measure. The distance measure f_{dis} represents the term $'c_2 R + c_3 \ln(R + c_4 exp(c_5 M))'$ corresponds to geometric and anelastic attenuation (equation 11). Since all the high amplitude records of the dataset are concentrated at distances less than 20 km from the source, near field magnitude saturation due to the M_w 7.9 mainshock is expected. In order to capture this property, the term

$'c_4\, exp(c_5 M)'$ is incorporated in the model; wherein these non-linear coefficients are obtained using non-linear least square regression analysis. The f_{site} represents the term $'c_6 F_{Vs30}'$ incorporating the local site conditions where $'F_{Vs30}'$ includes flags for the site classes as per V_s30 (equation 12). Further, it is already mentioned in the earlier sections that the sediment depth varies from 0.6-5 km in the IG basin, whereas the sediment thickness ranges between 0.04-0.46 km in the Kathmandu basin. Based on sediment thickness variation, the sites are classified into three different classes. The sites for sediment depth <1 is marked with F_{sed}=0; for sediment depth from 1 km to 2.5 km with F_{sed}=1; for sediment depth greater than 2.5 with F_{sed}=3. Therefore the term $'f_{sed}'$ incorporates site spectral amplification factor via the site's sediment depth (equation 13). The event-to-event (inter-event,η_i) and within event (intra-event,ϵ_{ij}) residuals are independent and identically distributed and are jointly normal (equation 14). The coefficients $c_k(k = 0,1, \dots,7)$ in the equation 8 and the corresponding inter-event and intra-event standard deviations are shown in table 7. The estimates thus obtained are plotted against recorded data for all the 21 GMPs in Fig. 12. It can be observed that the functional form considered in the study is able to capture the trend in the behavior of GMPs with source and distance measures. In order to evaluate the validity of the GMPE developed in this study, the inter-event and intra-event residuals obtained from the mixed effect regression analysis are plotted against the predictor variables in the model. The variation of the residuals plots are shown in Figure A7 (Electronic supplement). In these residual plots, a positive residual indicates the underestimation of the actual value by the predicted model and a negative residual indicates the overestimation of the actual value by the predicted model. It is observed that neither inter-event nor intra-event residuals shows trend with respect to the predictor variables.

5. COMPARISON WITH ESTABLISHED GMPES

In order to study the goodness of the model, the GMPEs developed here are compared with previously established GMPEs that were applicable to the region considered in this study (Douglas, 2020). Subsequently, a comparison of these already established models with the present model is presented for the two events of magnitudes M_w7.2 and M_w 7.9.

5.1. Peak Ground Acceleration (PGA)

Regionally established regression model proposed by Singh *et al.* (2017) – SSSA17 and well established global GMPEs proposed by ASK14 – Abrahamson et al. (2014), Boore *et al.* (2014) – BSSA14, Campbell and Bozorgnia (2014) – CB14, Chiou and Youngs (2014) – CY14, Kanno *et al.* (2006) – K06 and Zhao *et al.* (2006) – Z06, are selected for comparison of the GMPE derived for PGA. All the global models are derived for different tectonic environments. ASK14 developed the ground motion model for mean horizontal component of PGA for shallow crustal earthquakes in active tectonic regions, where the regression equations were developed using the NGA-West2 database. BSSA14 includes the GMPE for mean horizontal component of PGA, PGV and PSA (5 % damping ratio) for the same database. Similarly, CB14 was also developed for the NGA-West2 database, which includes

period-dependent magnitude saturation, faulting effects, magnitude-dependent scaling with hypocentral depth and fault dip, regionally dependent anelastic attenuation, updated hanging wall effects and so on. K06 includes two regression models for shallow and deep events with a V_s30 of 300m/s. Z06 includes attenuation models considering tectonic source types and focal mechanisms. SSSA17 was proposed for IGP based on an approximate solution of a circular finite source model using the same database. The GMPE is derived using exponential integral function where M_w and R_{rup} are considered as the predictor variables. Fig. 13 shows the comparison of different GMPEs with the PGA values estimated using a flag value of 2 for both F_{Vs30} and F_{sed} and for two moment magnitudes: M_w7.2 and M_w 7.9. It is observed from the figure that the global GMPEs are under-predicting the recorded data. It can be observed that the developed model is able to predict the data. Remarkably, the regional prediction model proposed by SSSA17 is able to capture the trend of the data. However, it can be observed from table 7 that the inter-event and intra-event standard deviation of the present model is lesser than that of SSSA17. Moreover, the present model also incorporates site classes and sediment depth variations along with the M_w and R_{rup} in the functional form. Thus, the GMPE derived in the present study provides better estimates compared to other models.

5.2. Peak Ground Velocity (PGV)

Similarly, regression models proposed by Singh *et al.* (2017) – SSSA17, ASK14 – Abrahamson et al. (2014), Boore *et al.* (2014) – BSSA14, Campbell and Bozorgnia (2014) – CB14, Chiou and Youngs (2014) – CY14, and Kanno *et al.* (2006) – K06 are compared with the GMPE derived for PGV. Consequently, corrections are applied to the model K06. Fig. 14 shows the comparison of these GMPEs, with the PGV estimated using a flag value of 2 for both F_{Vs30} and F_{sed} and for two moment magnitudes: M_w7.2 and M_w 7.9. The models BSSA14, CB14, and CY14 are under-predicting the records whereas estimates of SSSA17 and K06 are close to the present model and provides a sufficiently close estimation of PGV.

5.3. Peak Ground Displacement (PGD)

The models given by Singh *et al.* (2017) – SSSA17 and Campbell and Bozorgnia (2008) – CB08 are selected for the comparison of the GMPE derived for PGD. The model CB08 was derived for crustal events, and includes hypocentral depth, shallow linear and nonlinear site responses, 3-D basin response and hanging wall effects. Due to lack of information, the present model does not consider fault mechanisms and basin responses. Fig. 15 shows the comparison plot of the GMPEs using a flag value of 2 for both F_{Vs30} and F_{sed} and for magnitudes M_w7.2 and M_w 7.9. The model CB08 is over-predicting the estimated values of PGD, whereas the model SSSA17 gives sufficiently closer estimates to the recorded data.

5.4. Arias Intensity (I_a)

There are very few GMPEs available for complex parameters like arias intensity, root-mean-square acceleration and CAV. The GMPEs derived by Sharma and Srbulov (1998) – SS98, Foulser-Piggot and Goda (2014) – FPG14 and Amiri *et al.* (2009) – A09 are selected for the comparison of arias intensity (I_a). The model SS98 considered duration and number of pulses as a function of acceleration, in addition to the usual predictor variables like magnitude and

source-to-site distance. Further, surface wave magnitude (M_s) was used as source measure, and equations were derived for rock and soil site conditions. The model A09 also used surface wave magnitude to derive four different equations for different ground types and tectonic conditions for Iran. The comparison of these GMPEs with the present model for I_a using a flag value of 2 for both F_{Vs30} and F_{sed} is shown in Fig. 16. It is observed that the model A09 is not following the trend in the behaviour with predictor variables. However, the model SS98 is over-predicting the data for M_w 7.2 while able to follow the trend for M_w 7.9. FPG14 is under-predicting the arias intensity for far-field records and overestimating the same for near field records. As expected, the regression equation derived in the present study provides better estimates compared to other models.

5.5. Cumulative Absolute Velocity (CAV)

In this section, models proposed by Campbell and Bozorgnia (2010) – CB10, Foulser-Piggot and Goda (2014) – FPG14 and Du and Wang (2013) – DW13 are used to compare the estimates of CAV. The models CB10 and DW13 include intercontinental ground motions to derive prediction equations for shallow crustal events. These models incorporate magnitude, source-to-site distance, site conditions, faulting style hanging wall effect, linear and nonlinear site response. However, both the models are not following the trend in the behaviour of parameters and gives under-predicting estimates for CAV values. However, the model FPG14 provides sufficiently close estimates of CAV for far-field data while overestimating the near field data. Fig. 17 shows that the present model is relatively good in predicting the estimates.

6. RANKING OF GMPES

Since the model derived in the current study used a limited dataset of ground motion records, the GMPEs cannot be used directly in any hazard studies. With the advent of statistical approaches such as the likelihood methods, the goodness of GMPEs can be quantified such that the most suitable model for a particular region can be selected with more ease. Therefore, a statistical analysis is performed to facilitate the ranking of the established GMPEs hierarchically for hazard and risk assessment. The most popular methods for this task are the likelihood (LH) method (Scherbaum *et al.,* 2004), the log-likelihood (LLH) method (Scherbaum *et al.*, 2009) and the Euclidean distance (EDR) method (Kale and Akkar 2013). The basic concept in the LH method involves normalization of residuals obtained between the recorded data and estimates, with standard deviation of the GMPE. The LLH method measures the average log likelihood of the estimates given by the GMPE and the observed data, both of which are considered as two continuous log normal probability density functions. On the other hand, the EDR method makes use of the Euclidean distance concept to obtain raking of various GMPEs. All the above three methods may sometimes give different rankings for a set of GMPEs, as the LH method is sensitive to standard deviations. Therefore, the concept of normalized ranking index (RI_N) is opted here, which is obtained from using all the above three methods to derive an unbiased ranking system for the GMPEs (Kale, 2009). Table 8 gives the ranks obtained for all the GMPEs considered for comparison

of PGA in this study, using all the three statistical methods. It can be observed that the all the GMPEs are placed in a different ranking order for each of the methods. Similar observations are noticed in the cases of PGV, PGD, I_a and CAV, which are given in tables 9-12 respectively. Therefore the ranking indices are normalized for each method, by giving the best performing GMPE a value of 1.0. Further, the final normalized ranking index (RI_N) is obtained by taking a weighted combination (EDR-0.50, LH-0.25 and LLH-0.25) of the corresponding normalized rankings (EDR_N, LH_N and LLH_N).

The final ranks thus obtained for the GMPEs of PGA, PGV, PGD, I_a and CAV are given in tables 13 and 14 respectively. From the tables, it can be observed that the model derived in the present study is ranked at number one for all the GMPs, the reason being the calibration of the model exclusively to the recorded data used in this study. On that note, it can also be observed that the other locally derived model SSSA17 is ranked at number 2 for PGA and PGD. All the other global models register much higher RI_N values for PGA, verifying that the Nepal earthquake is a truly unique event of the Himalayan tectonic zone, which cannot be estimated effectively by many well established global models. Interestingly, the RI_N values are much less for PGV and PGD, especially the K06 model that is derived for Japan, which signifies that either some of the global models are effective in predicting these parameters or that the current model still needs improvisation. The same pattern can be obtained from the plots given in figures 13, 14 and 15. The rankings obtained for I_a and CAV also follows the same pattern as observed from the plots of figures 16 and 17.

7. CONCLUSION

The 2015 M_w 7.9 Nepal earthquake is not only the most catastrophic but also the first well-recorded event to have occurred in the Himalayan orogenic belt. This paper presents a detailed analysis of this event using 21 GMPs, which represents the amplitude, frequency content, duration and evolutionary characteristics of the ground motion. Preliminary analysis indicates that very low PGA values are recorded wherein the near field station KTP, which is located on a rock site with an R_{rup} of 12.05 km has recorded PGA of 0.265g. However, the a_{RMS} value for this ground motion record is lower to that of others that were recorded on sediment sites located at similar rupture distances. This behaviour is also seen in other second order parameters of the Kathmandu basin. Moreover, analysis of spectral accelerations emphasizes the presence of long period spectral amplitudes in near field ground motions of Kathmandu basin, only at sediment sites. However, the same pattern is not observed in the far field IG basin records of the earthquake. Therefore, a thorough study of the ground motion characteristics through first, second and third order GMPs is conducted.

The behaviour of the parameters concerning the thickness of sediment is studied through IMFs using HHT-EMD for all the ground motions of the M_w 7.9 earthquake. Interestingly, the IMFs with higher modes become predominant as the thickness of sediments in the IG basin increases from south to north, thereby resulting in low dominant mean instantaneous frequencies for sites having larger sediment depths. Moreover, for the station KTP located at

a hard rock site of Kathmandu basin, maximum percentage variance is observed for the first IMF; whereas higher order (third to sixth) IMFs are more dominant for sediment sites (PTN, THM, TVU and KATNP). Therefore, a similar pattern is observed for both the Kathmandu and IG basins with respect to dominant mean frequencies and sediment depths. Lack of any noticeable predominant long period spectral amplitude for most of the records in the IG basin is attributed to the overall low amplitudes resulting from the source mechanism, combined with large rupture distances. The effect of sediment depth on ground motions over short and long time periods is emphasised more through the HHT-based site amplification study. A significant increase is observed in the amplification values at the dominant frequencies for HHT- based method than the Fourier based method. Comparing the M_w 7.9 mainshock with two of its aftershocks, the increased site amplification at lower frequencies for the higher magnitude events can be considered as an indication of soil nonlinearity at these sites. Remarkably, the station VNS with much lesser sediment depth compared to the other sites shows weak or no site nonlinearity under the mainshock. However, a denser dataset would provide in a visibly comprehensible pattern.

Additionally, in this study, GMPEs are derived for the 21 estimated GMPs, using nonlinear mixed effect regression analysis to incorporate both fixed and random effects. The predictor variables used for deriving GMPEs are Moment Magnitude (M_w), Rupture distance (R_{rup}), flags for Vs30 of the site (F_{Vs30}) and sediment depth variation (F_{sed}).The estimates thus obtained from the GMPE are compared with the recorded values of the M_w 7.9 mainshock and the M_w 7.2 aftershock records. Further, to ensure that the developed GMPEs are not biased, the behaviour of inter-event and intra-event residuals against the predictor variables is verified. Furthermore, the estimated GMPEs are compared with well established prediction models that can be applicable to the study region. Among the few models applicable to parameters such as PGA, PGV, PGD, I_a and CAV, superior prediction is observed from the estimates of the current model. Similar class of estimates can be expected for all the second and third order GMPs of the current model, which is a novel endeavour for the Nepal Himalaya region. In addition, the evaluation of ranking indices (RI_N) also highlights the efficiency of the current model. Since all the earthquakes considered in this study are originated due to a similar source mechanism, the GMPE model given here is not only region specific, but also source specific. Analysis using a wide range of data would further ensure the goodness of this model and its applicability. The GMPEs developed in this study may not be used directly in applications such as PSHA studies due to the constricted dataset used in deriving the models. However, when used with a logic tree approach, all the GMPEs will contribute quite significantly. Further, the GMPEs of higher order parameters can be even used to generate ground motion time-histories using stochastic methods such as the one given by Sabetta and Pugliese (2021), which can be used for a nonlinear dynamic analysis in earthquake-resistant design.

8. REFERENCES

706 Abrahamson, N.A. and Youngs, R.R., [1992].A stable algorithm for regression analyses using the
707 random effects model. *Bulletin of the Seismological Society of America*, *82*(1), pp.505-510.

708 Abrahamson, N.A., Silva, W.J. and Kamai, R., [2014]. Summary of the ASK14 ground motion
709 relation for active crustal regions. *Earthquake Spectra*, *30*(3), pp.1025-1055.

710 A. Joshi, A. Kumar, K. Mohran, and B. K. Rastogi. Hybrid attenuation model for estimation of peak
711 ground accelerations in the Kutch region, India. Natural Hazards, 68(2):249269, [2013b]. doi:
712 10.1007/ s11069-012-0524-7

713 Amiri, G.G., Khorasani, M., Hessabi, R.M. and Amrei, S.R., [2009].Ground-motion prediction
714 equations of spectral ordinates and Arias intensity for Iran. *Journal of Earthquake Engineering*, *14*(1),
715 pp.1-29

716 Ang, A.H.S., [1990]. Reliability bases for seismic safety assessment and design. In Proceedings,
717 Fourth National Conference on Earthquake Engineering, EERI, pp. 29-45.

718 Arias A. [1970], "A measure of earthquake intensity", Seismic Design for Nuclear Power Plants.
719 Hansen RJ (Ed.), MIT Press, Cambridge: 438–483.

720 Bajaj, K. and Anbazhagan, P., [2019]. Seismic site classification and correlation between VS and
721 SPT-N for deep soil sites in Indo-Gangetic Basin. *Journal of Applied Geophysics*, *163*, pp.55-72.

722 Benioff, H., [1934]. The physical evaluation of seismic destructiveness. *Bulletin of the Seismological*
723 *Society of America*, *24*(4), pp.398-403.

724 Bhargavi, P. and Raghukanth, S.T.G., [2019a]. Ground motion parameters for the 2011 Great Japan
725 Tohoku earthquake. *Journal of Earthquake Engineering*, *23*(4), pp.688-723.

726 Bhargavi, P. and Raghukanth, S.T.G., [2019b]. Rating damage potential of ground motion
727 records. *Earthquake Engineering and Engineering Vibration*, *18*(2), pp.233-254.

728 Bijukchhen, S.M., Takai, N., Shigefuji, M., Ichiyanagi, M., Sasatani, T. and Sugimura, Y., [2017].
729 Estimation of 1-D velocity models beneath strong-motion observation sites in the Kathmandu Valley
730 using strong-motion records from moderate-sized earthquakes. *Earth, Planets and Space*, *69*(1), pp.1-
731 16.

732 Boore, D. M., Stewart, J. P., Seyhan, E., & Atkinson, G. M. [2014]. NGA-West2 equations for
733 predicting PGA, PGV, and 5% damped PSA for shallow crustal earthquakes. Earthquake Spectra,
734 30(3), 1057-1085.

735 Campbell, K.W. and Bozorgnia, Y., [2008]. NGA ground motion model for the geometric mean
736 horizontal component of PGA, PGV, PGD and 5% damped linear elastic response spectra for periods
737 ranging from 0.01 to 10 s. *Earthquake Spectra*, *24*(1), pp.139-171

738 Campbell, K.W. and Bozorgnia, Y., [2010]. A ground motion prediction equation for the horizontal
739 component of cumulative absolute velocity (CAV) based on the PEER-NGA strong motion
740 database. *Earthquake Spectra*, *26*(3), pp.635-650.

741 Campbell, K. W., &Bozorgnia, Y. [2014]. NGA-West2 ground motion model for the average
742 horizontal components of PGA, PGV, and 5% damped linear acceleration response spectra.
743 Earthquake Spectra, 30(3), 1087-1115.

Center for Engineering Strong Motion Data (CESMD), http://www.strongmotioncenter.org/

Chadha, R.K., Srinagesh, D., Srinivas, D., Suresh, G., Sateesh, A., Singh, S.K., Pérez-Campos, X., Suresh, G., Koketsu, K., Masuda, T. and Domen, K., [2016]. CIGN, a strong-motion seismic network in central Indo-Gangetic plains, foothills of Himalayas: First results. *Seismological Research Letters*, *87*(1), pp.37-46.

Chiou, B. S. J., &Youngs, R. R., [2014]. Update of the Chiou and Youngs NGA model for the average horizontal component of peak ground motion and response spectra. Earthquake Spectra, 30(3), 1117-1153.

Dhakal, Y.P., Kubo, H., Suzuki, W., Kunugi, T., Aoi, S. and Fujiwara, H., [2016].Analysis of strong ground motions and site effects at Kantipath, Kathmandu, from 2015 Mw 7.8 Gorkha, Nepal, earthquake and its aftershocks. *Earth, Planets and Space*, *68*(1), pp.1-12.

Dhanya, J., Gade, M. and Raghukanth, S.T.G., [2017].Ground motion estimation during 25th April 2015 Nepal earthquake. *ActaGeodaeticaetGeophysica*, *52*(1), pp.69-93.

Douglas, J. [2020]. Ground motion prediction equations 1964–2019.http://www.gmpe.org.uk.

Du, W. and Wang, G., [2013].A simple ground-motion prediction model for cumulative absolute velocity and model validation. *Earthquake engineering & structural dynamics*, *42*(8), pp.1189-1202.

Electrical Power Research Institute (EPRI), [1988], "A Criterion for Determining Exceedance of the Operating Basis Earthquake", EPRI NP-5930, Palo Alto, CA.

Foulser-Piggott, R. and Goda, K., [2014], August.New prediction equations of Arias intensity and cumulative absolute velocity for Japanese earthquakes.In *Second Eurpoean Conference on Earthquake Engineering and Seismology* (pp. 1-11).

Galetzka, J., Melgar, D., Genrich, J.F., Geng, J., Owen, S., Lindsey, E.O., Xu, X., Bock, Y., Avouac, J.P., Adhikari, L.B. and Upreti, B.N., [2015]. Slip pulse and resonance of the Kathmandu basin during the 2015 Gorkha earthquake, Nepal. *Science*, *349*(6252), pp.1091-1095.

Gansser, A., [1964]. Geology of the Himalayas.

Goda, K., Kiyota, T., Pokhrel, R.M., Chiaro, G., Katagiri, T., Sharma, K. and Wilkinson, S., [2015]. The 2015 Gorkha Nepal earthquake: insights from earthquake damage survey. *Frontiers in Built Environment*, *1*, p.8.

Grandin, R., Vallée, M., Satriano, C., Lacassin, R., Klinger, Y., Simoes, M. and Bollinger, L., [2015]. Rupture process of the Mw= 7.9 2015 Gorkha earthquake (Nepal): Insights into Himalayan megathrust segmentation. *Geophysical Research Letters*, *42*(20), pp.8373-8382.

Hayes, G.P., Briggs, R.W., Barnhart, W.D., Yeck, W.L., McNamara, D.E., Wald, D.J., Nealy, J.L., Benz, H.M., Gold, R.D., Jaiswal, K.S. and Marano, K., [2015]. Rapid characterization of the 2015 M w 7.8 Gorkha, Nepal, earthquake sequence and its seismotectonic context. *Seismological Research Letters*, *86*(6), pp.1557-1567.

Housner, G.W., [1952]. Spectrum intensities of strong-motion earthquakes

Housner, G.W. and Jennings, P.C., [1964]. Generation of artificial earthquakes. *Journal of the Engineering Mechanics Division*, *90*(1), pp.113-152.

Huang, N.E., Shen, Z., Long, S.R., Wu, M.C., Shih, H.H., Zheng, Q., Yen, N.C., Tung, C.C. and Liu, H.H., [1998]. The empirical mode decomposition and the Hilbert spectrum for nonlinear and non-stationary time series analysis. *Proceedings of the Royal Society of London. Series A: mathematical, physical and engineering sciences*, *454*(1971), pp.903-995.

Husid R.L. [1969]. Analisis de terremotos: Analisis General, Revista del IDIEM 8:1, Universidad de Chile,Santiago, Chile, 21-42.

Iyengar, R.N. and Kanth, S.R., 2006. Strong ground motion estimation during the Kutch, India earthquake. *Pure and applied geophysics*, *163*(1), pp.153-173.

Kale, Ö., [2019]. Some discussions on data-driven testing of Ground-Motion Prediction Equations under the Turkish ground-motion database. *Journal of Earthquake Engineering*, *23*(1), pp.160-181.

Kale, Ö. and Akkar, S., [2013]. A new procedure for selecting and ranking ground-motion prediction equations (GMPEs): The Euclidean distance-based ranking (EDR) method. *Bulletin of the Seismological Society of America*, *103*(2A), pp.1069-1084.

Kanno, T., Narita, A., Morikawa, N., Fujiwara, H. and Fukushima, Y., [2006]. A new attenuation relation for strong ground motion in Japan based on recorded data. *Bulletin of the Seismological Society of America*, *96*(3), pp.879-897.

Kanth, S.R. and Iyengar, R.N., 2007. Estimation of seismic spectral acceleration in peninsular India. *Journal of Earth System Science*, *116*(3), pp.199-214.

Koketsu, K., Miyake, H., Guo, Y., Kobayashi, H., Masuda, T., Davuluri, S., Bhattarai, M., Adhikari, L.B. and Sapkota, S.N., [2016].Widespread ground motion distribution caused by rupture directivity during the 2015 Gorkha, Nepal earthquake. *Scientific reports*, *6*(1), pp.1-9.

Kramer, S.L., [1996]. *Geotechnical earthquake engineering*. Pearson Education India

Kumar, A., Mittal, H., Sachdeva, R. and Kumar, A., [2012].Indian strong motion instrumentation network. *Seismological Research Letters*, *83*(1), pp.59-66.

Liu, S.C., [1970]. Evolutionary power spectral density of strong-motion earthquakes. *Bulletin of the Seismological Society of America*, *60*(3), pp.891-900.

Nath, S.K., Vyas, M., Pal, I., Singh, A.K., Mukherjee, S. and Sengupta, P.,[2005]. Spectral attenuation models in the Sikkim Himalaya from the observed and simulated strong motion events in the region. *Current Science*, pp.295-303.

Nath, S.K., Thingbaijam, K.K.S., Maiti, S.K. and Nayak, A., [2012]. Ground-motion predictions in Shillong region, northeast India. *Journal of seismology*, *16*(3), pp.475-488.

Park, Y.J. and Ang, A.H.S., [1985]. Mechanistic seismic damage model for reinforced concrete. *Journal of structural engineering*, *111*(4), pp.722-739.

Priestley, M.B., [1965]. Evolutionary spectra and non-stationary processes. *Journal of the Royal Statistical Society: Series B (Methodological)*, *27*(2), pp.204-229.

817 Rajaure, S., Asimaki, D., Thompson, E.M., Hough, S., Martin, S., Ampuero, J.P., Dhital, M.R., Inbal,
818 A., Takai, N., Shigefuji, M. and Bijukchhen, S., [2017]. Characterizing the Kathmandu Valley
819 sediment response through strong motion recordings of the 2015 Gorkha earthquake
820 sequence. *Tectonophysics*, *714*, pp.146-157.

821 Raghukanth, S.T.G. and Sangeetha, S., [2012]. Empirical mode decomposition of earthquake
822 accelerograms. *Advances in Adaptive Data Analysis*, *4*(04), p.1250022.

823 Reed, J.W. and Kassawara, R.P., [1990]. A criterion for determining exceedance of the operating
824 basis earthquake. *Nuclear Engineering and Design*, *123*(2-3), pp.387-396.

825 Sabetta, F., Pugliese, A., Fiorentino, G., Lanzano, G. and Luzi, L., 2021. Simulation of non-stationary
826 stochastic ground motions based on recent Italian earthquakes. *Bulletin of Earthquake Engineering*,
827 pp.1-29.

828 Sakai, H., Fujii, R. and Kuwahara, Y., [2002]. Changes in the depositional system of the Paleo-
829 Kathmandu Lake caused by uplift of the Nepal Lesser Himalayas. *Journal of Asian Earth*
830 *Sciences*, *20*(3), pp.267-276.

831 Scherbaum, F., Cotton, F. and Smit, P., [2004]. On the use of response spectral-reference data for the
832 selection and ranking of ground-motion models for seismic-hazard analysis in regions of moderate
833 seismicity: The case of rock motion. *Bulletin of the seismological society of America*, *94*(6), pp.2164-
834 2185.

835 Scherbaum, F., Delavaud, E. and Riggelsen, C., [2009]. Model selection in seismic hazard analysis:
836 An information-theoretic perspective. *Bulletin of the Seismological Society of America*, *99*(6),
837 pp.3234-3247.

838 Sarma, S.K. and Srbulov, M., [1998].A uniform estimation of some basic ground motion
839 parameters. *Journal of Earthquake Engineering*, *2*(02), pp.267-287.

840 Sharma, M.L., Douglas, J., Bungum, H. and Kotadia, J., [2009]. Ground-motion prediction equations
841 based on data from the Himalayan and Zagros regions. *Journal of Earthquake Engineering*, *13*(8),
842 pp.1191-1210.

843 Singh, S.K., Srinagesh, D., Pérez-Campos, X., Srinivas, D., Suresh, G., Suresh, G. and Chadha, R.K.,
844 [2020]. Seismic wave amplification in the central Indo-Gangetic Plains, India, estimated from the
845 ratio of soft to hard site source spectrum. *Journal of Seismology*, pp.1-14.

846 Singh, S.K., Srinagesh, D., Srinivas, D., Arroyo, D., Pérez-Campos, X., Chadha, R.K., Suresh, G. and
847 Suresh, G., [2017].Strong Ground Motion in the Indo-Gangetic Plains during the 2015 Gorkha, Nepal,
848 Earthquake Sequence and Its Prediction during Future Earthquakes. *Bulletin of the Seismological*
849 *Society of America*, *107*(3), pp.1293-1306.

850 Srinagesh, D., Singh, S.K., Chadha, R.K., Paul, A., Suresh, G., Ordaz, M. and Dattatrayam, R.S.,
851 [2011].Amplification of seismic waves in the central Indo-Gangetic basin, India. *Bulletin of the*
852 *Seismological Society of America*, *101*(5), pp.2231-2242.

853 Takai, N., Shigefuji, M., Rajaure, S., Bijukchhen, S., Ichiyanagi, M., Dhital, M.R. and Sasatani, T.,
854 [2016]. Strong ground motion in the Kathmandu Valley during the 2015 Gorkha, Nepal,
855 earthquake. *Earth, Planets and Space*, *68*(1), pp.1-8.

USGS [2015b] NetQuakes: Station KATNP_NQ_01, 25 April 2015. http://earthquake.usgs.gov/monitoring/netquakes/station/KATNP_NQ_01/20150425061138/.

Valdiya, K.S., [1964]. The unfossiliferous formations of the Lesser Himalaya and their correlation.In *22nd International Geological Congress.''Delhi* (pp. 15-36).

Vanmarcke, E.H., [1976]. Structural response to earthquakes.In *Developments in Geotechnical Engineering* (Vol. 15, pp. 287-337).Elsevier.

Von Thun, J.L., [1988]. Earthquake ground motions for design and analysis of dams. *Earthquake engineering and soil dynamics II-recent advances in ground-motion evaluation*.

Wu, Z. and Huang, N.E., [2009]. Ensemble empirical mode decomposition: a noise-assisted data analysis method. *Advances in adaptive data analysis*, *1*(01), pp.1-41.

Zhang, R.R., [2006]. Characterizing and quantifying earthquake-induced site nonlinearity. *Soil Dynamics and Earthquake Engineering*, *26*(8), pp.799-812.

Zhao, J.X. and Lu, M., [2011].Magnitude-Scaling Rate in Ground-Motion Prediction Equations for Response Spectra from Large, Shallow Crustal Earthquakes. *Bulletin of the Seismological Society of America*, *101*(6), pp.2643-2661.

873 **Table 1.** Earthquake ground motion database used in the current study

Sl. No:	Name of the Earthquake	Date (Day/mon/year)	Time (hr:min)	Epicenter		Depth (km)	M_w	No. of Records
				Lat (^oE)	Lon (^oN)			
1	Mainshock	25-04-2015	06:11	27.92	85.325	12	7.9	32
2	Aftershock 1	25-04-2015	06:45	28.224	84.822	21	6.7	23
3	Aftershock 2	26-04-2015	07:09	27.771	86.017	20.6	6.7	25
4	Aftershock 3	12-05-2015	07:05	27.809	86.066	12	7.2	25
5	Aftershock 4	12-05-2015	07:36	27.625	86.162	18.1	6.2	26
4	Aftershock 5	16-05-2015	11:34	27.559	86.078	12	5.3	24

874

875 **Table 2.** Site classification based on Vs30 ranges, as proposed by the International Building
876 Code (IBC 2009)

Soil shear wave velocity, V_s30 (m/s)	Soil Type	Site Class	Flag used in the model
V_s30 >1500	Hard Rock	A	0
760< V_s30 ≤1500	Rock	B	1
360< V_s30 ≤760	Soft Rock	C	2
180≤ V_s30 ≤360	Stiff soil	D	3
V_s30 <180	Soft soil	E	4

877

878 **Table 3.** Details of ground motion recording stations used in the present study.

Sl. No.	Station				Sediment Depth (km)	Network	Site class
	Name	Code	Lat (°E)	Lon (°N)			
1	Agra	AGR	27.1607	78.0192	0.6	CIGN	D
2	Allahabad	ALB	25.1257	82.125	0.9	CIGN	C
3	Aligarh	ALG	27.9709	77.7888	0.6	CIGN	D
4	Almora	ALM	29.5478	79.5488	5	CIGN	D
5	Amethi	AMT	26.1878	81.679	1.2	CIGN	C
6	Bagaha	BAG	27.137	84.06	4	IITR	C
7	Balrampur	BRP	27.505	82.0556	5	CIGN	C
8	Bisalpur	BSR	28.2098	79.8053	3.6	CIGN	D
9	Chandigarh	CDG	30.7609	76.7674	4.4	CIGN	C
10	Faizabad	FZB	26.7308	82.1467	3.1	CIGN	D
11	Gonda	GDA	27.1162	82.2371	2.7	CIGN	D
12	Gorakhpur	GRP	26.9504	83.3167	4.7	CIGN	D
13	Hardoi	HAR	27.396	80.133	2.9	IITR	D
14	Haridwar	HDR	29.9752	78.0529	3.7	CIGN	D
15	Hisar	HSR	29.445	75.608	1	CIGN	D
16	Jaunpur	JAU	25.733	82.693	1	IITR	E
17	Kanti Path	KATNP	27.712	85.316	0.47	USGS	D
18	Kanpur	KNP	26.2694	80.5007	0.6	CIGN	C
19	Kishanganj	KSN	26.095	87.947	4	IITR	C
20	Kirtipur	KTP	27.682	85.272	0.04	CESMD	C
21	Kushinagar	KUS	26.865	83.957	3.5	IITR	E
22	Lakhimpur	LAK	27.949	80.79	4	IITR	C
23	Loharpur	LEH	27.709	80.89	3.5	IITR	C
24	Maharajganj	MAH	27.141	83.539	4	IITR	C
25	Meerut	MRT	29.1542	77.6178	2.5	CIGN	D
26	Motihari	MTR	26.63	84.899	2.5	CIGN	D
27	Narora	NAR	28.227	78.4256	1.7	CIGN	D
28	Pihani	PHN	27.6506	80.1606	3.6	CIGN	D
29	Patan(IGP)	ptn	25.622	85.149	1	IITR	E
30	Patan(KB)	PTN	27.681	85.318	0.35	CESMD	D
31	Rath	RAT	25.6261	79.5722	0.7	CIGN	B
32	Raibarely	RBL	26.3633	81.2694	1.2	CIGN	D
33	Rudraprayag	RPG	30.5463	79.0634	5	CIGN	D
34	Sikandrarao	SDR	27.7388	78.4739	1.6	CIGN	D
35	Thakurdwara	TDR	29.1489	78.8551	4.6	CIGN	D
36	Sanothimi	THM	27.681	85.377	0.46	CESMD	D
37	Tarikhet	TKT	29.6132	79.4047	5	CIGN	D
38	Tribhuvan University	TVU	27.681	85.288	0.325	CESMD	D
39	Utraula	UTR	27.31	82.415	3.5	IITR	C
40	Varanasi	VNS	25.5536	82.8541	0.7	CIGN	D

879

880 **Table 4.** Basic definitions of Ground Motion Parameters estimated in this study.

Sl. No.	Ground Motion Parameter	Mathematical expression	Key characteristics
1.	Peak Ground Acceleration (PGA)	PGA = max(abs(a(t))) a(t) – acceleration time history	Amplitude
2.	Peak Ground Velocity (PGV)	PGA = max(abs(V(t))) V(t) =	Amplitude
3.	Peak Ground Displacement (PGD)	PGA = max(abs(a(t))) a(t) – acceleration time history	Amplitude
4.	Vertical to Horizontal, V/H (PGA)	PVA/PHA	Amplitude
5.	Predominant Frequency, F_p	Frequency corresponding to max(fft(a(t))) fft(a(t)) – Fourier amplitude spectrum	Frequency content
6.	Central Frequency, Ω	$\Lambda n = \int_0^{\omega N} \omega^n G(\omega)\ d\omega$ $\Omega = \sqrt{\frac{\lambda 2}{\lambda 0}}$ $G(\omega)$- Power Spectral Density	Frequency content
7.	Shape factor, q	$q = \sqrt{1 - \frac{\lambda^2}{\lambda 0\ \lambda 2}}$	Frequency content
8.	Velocity to Acceleration ratio, V/A	PGV/PGA	Frequency content
9.	Significant duration, T_{sig}	Tsig= T5−95%([a(t)]^2)	Duration
10.	Root-Mean-Square Acceleration, a_{RMS}	$\alpha_{RMS} = \sqrt{\frac{1}{Tsig}\int_{t1}^{t2}[a(t)^2\ dt}$	Amplitude, Frequency content
11.	Arias Intensity, I_a	$I_a = \frac{\pi}{2g}\int_0^{\infty}[a(t)]^2\ dt$	Amplitude, Frequency content, Duration
12.	Cumulative Absolute Velocity, CAV	$\mathrm{CAV} = \int_0^{Tsig} \lvert a(t) \rvert\ dt$	Amplitude, Frequency content, Duration
13.	Characteristic Intensity, I_c		Amplitude, Frequency content, Duration
14.	Acceleration Spectrum Intensity, ASI	$\mathrm{ASI} = \int_{0.1}^{0.5} PSA(\varepsilon_v = 0.05, T)\ dT$	Amplitude, Frequency content

15.	Velocity Spectrum Intensity, VSI	$\text{VSI} = \int_{0.1}^{2.5} PSV(\varepsilon_u = 0.05, T)\, dT$	Amplitude, Frequency content
16.	Total Energy, E_{acc}	$E_{acc} = \int_0^{\infty}\int_0^{\infty} G(t,\omega)d\omega dt$	Amplitude, Frequency content, Duration
17.	Spectral Centroid, E_w	$E_w(\omega) = \frac{\int_{t_1}^{t_2}\int_0^{N_{yq}} \omega G(t,\omega)d\omega dt}{\int_{t_1}^{t_2}\int_0^{N_{yq}} G(t,\omega)\, d\omega dt}$	
18.	Spectral Standard deviation, S_w	$S_w{}^2(\omega) = \frac{\int_{t_1}^{t_2}\int_0^{N_{yq}} [\omega - E(\omega)]^2 G(t,\omega)d\omega dt}{\int_{t_1}^{t_2}\int_0^{N_{yq}} G(t,\omega)d\omega dt}$	
19.	Temporal Centroid, E_t	$E_t(t) = \frac{\int_{t_1}^{t_2}\int_0^{N_{yq}} tG(t,\omega)d\omega dt}{\int_{t_1}^{t_2}\int_0^{N_{yq}} G(t,\omega)\, d\omega dt}$	
20.	Temporal Standard deviation, S_t	$S_t{}^2(t) = \frac{\int_{t_1}^{t_2}\int_0^{N_{yq}} [t - E(t)]^2 G(t,\omega)d\omega dt}{\int_{t_1}^{t_2}\int_0^{N_{yq}} G(t,\omega)d\omega dt}$	
21.	Correlation between time and frequency, $\rho(\omega,t)$	$\rho(\omega,t) = \frac{\int_{t_1}^{t_2}\int_0^{N_{yq}} [t - E(t)][\omega - E(\omega)]G(t,\omega)d\omega dt}{S(t)S(\omega)\int_{t_1}^{t_2}\int_0^{N_{yq}} G(t,\omega)d\omega dt}$	

881

Table 5. Ground motion parameters obtained for strong motion records of two near field stations Kirtipur(KTP), Sanothimi (THM) and one IGP station Amethi (AMT): H-horizontal and V-vertical components.

Sl. No.	GMP	Unit	GROUND MOTION CHARACTERISTICS					
			KTP		THM		AMT	
			H	V	H	V	H	V
1	PHA	g	0.209	0.141	0.142	0.185	0.016	0.010
2	PHV	cm/s	30.13	29.998	63.596	41.651	3.386	1.340
3	PHD	cm	27.857	31.540	59.137	34.595	1.241	0.646
4	F_p	s^{-1}	0.153	0.216	0.459	0.229	0.215	0.138
5	CF	Hz	4.690	9.901	1.334	6.965	4.148	8.566
6	q	-	3.575	0.280	0.245	0.290	0.716	0.897
7	V/A	s	0.554	0.565	0.874	0.689	0.638	0.575
8	T_{sig}	s	37.984	40.959	40.637	36.253	97.85	109.8
9	a_{RMS}	g	0.033	0.023	0.045	0.032	0.004	0.002
10	I_a	cm/s	70.872	37.495	140.545	64.826	2.138	0.772
11	CAV	cm/s	890.17	694.285	1429.97	842.47	252.5	167.8
12	I_c	$\sqrt{cm^3 s^{-5}}$	1131.0	691.25	1865.28	1074.40	64.90	29.38
13	V/H	-	0.677		1.307		0.612	
14	ASI	cm/s	192.18	103.314	97.490	152.518	16.40	7.973
15	VSI	cm	64.663	52.933	139.835	92.841	9.901	4.782
16	E_{acc}	cm/s	140.88	37.857	312.318	72.288	4.351	0.763
17	E_w	Hz	3.552	7.592	0.541	4.578	2.893	6.666
18	S_w	Hz	2.523	5.596	1.430	4.776	2.584	5.031
19	E_t	s	40.444	38.416	46.178	39.918	239.4	230.4
20	S_t	s	12.836	13.325	12.762	11.755	59.53	71.44
21	ρ	-	0.196	0.013	0.0003	0.016	-0.01	-0.031

886 **Table 6.** Instantaneous frequency of the IMFs in Hz with mean – μ and standard deviation –
887 σ and respective percentage variances contributing to the total variability of the data.

Station Code			IMF1	IMF2	IMF3	IMF4	IMF5	IMF6	IMF7	IMF8	IMF9	IMF10
ALB	IF	μ	19.70	9.628	4.966	2.513	1.232	0.570	0.245	0.127	0.068	0.031
		σ	±6.78	±3.68	±2.07	±1.32	±0.71	±0.42	±0.22	±0.11	±0.04	±0.03
		% Var	32.79	27.23	14.72	12.52	7.497	2.860	1.660	0.238	0.111	0.048
VNS	IF	μ	16.58	7.300	3.687	1.903	0.877	0.397	0.183	0.096	0.051	0.025
		σ	±8.59	±3.72	±2.03	±1.14	±0.65	±0.33	±0.15	±0.06	±0.04	±0.02
		% Var	52.43	24.38	12.16	3.927	2.713	1.403	0.205	0.038	0.015	0.012
BRP	IF	μ	17.51	7.979	3.407	1.991	0.881	0.274	0.134	0.083	0.042	0.018
		σ	±7.95	±4.01	±2.26	±1.12	±0.62	±0.29	±0.08	±0.09	±0.03	±0.02
		% Var	23.97	32.65	26.16	10.45	4.750	1.426	0.306	0.050	0.038	0.016
GDA	IF	μ	17.48	7.720	3.703	1.645	0.882	0.256	0.140	0.081	0.043	0.019
		σ	±6.65	±3.74	±2.17	±1.27	±0.68	±0.26	±0.09	±0.05	±0.03	±0.02
		% Var	29.45	21.76	24.84	15.16	8.298	2.354	0.432	0.076	0.100	0.046
FZB	IF	μ	17.70	7.489	3.795	1.862	0.881	0.279	0.151	0.076	0.050	0.021
		σ	±7.99	±4.29	±1.94	±1.17	±0.69	±0.28	±0.08	±0.11	±0.09	±0.02
		% Var	29.14	30.67	22.64	10.12	4.240	2.579	0.630	0.184	0.019	0.017
AMT	IF	μ	19.04	8.486	3.775	2.094	0.920	0.349	0.184	0.097	0.044	0.027
		σ	±7.69	±4.20	±2.35	±1.25	±0.74	±0.33	±0.15	±0.12	±0.07	±0.02
		% Var	24.72	24.72	21.33	18.02	5.654	4.030	0.620	0.276	0.099	0.010
RAT	IF	μ	18.92	8.806	4.244	2.049	1.139	0.540	0.239	0.116	0.067	0.033
		σ	±7.23	±3.99	±2.22	±1.16	±0.56	±0.36	±0.19	±0.06	±0.04	±0.02
		% Var	26.67	24.69	44.79	4.426	0.985	0.356	0.153	0.113	0.036	0.022
NAR	IF	μ	22.83	10.72	5.059	2.479	1.200	0.435	0.218	0.111	0.058	0.029
		σ	±7.67	±5.10	±2.65	±1.33	±0.83	±0.44	±0.16	±0.09	±0.05	±0.02
		% Var	24.77	36.14	19.63	8.836	3.579	1.979	0.536	0.080	0.053	0.014
PHN	IF	μ	20.18	9.488	4.640	2.195	0.991	0.340	0.159	0.096	0.045	0.026
		σ	±7.60	±4.47	±2.26	±1.41	±0.84	±0.35	±0.15	±0.08	±0.03	±0.02
		% Var	27.94	27.62	18.05	10.69	6.264	5.163	1.364	0.206	0.057	0.020
BSR	IF	μ	20.00	9.475	4.318	2.138	0.896	0.281	0.140	0.077	0.048	0.021
		σ	±7.30	±4.49	±2.52	±1.37	±0.79	±0.29	±0.12	±0.06	±0.03	±0.02
		% Var	17.96	24.25	21.65	11.88	10.38	9.778	3.494	0.258	0.047	0.022
ALM	IF	μ	19.42	9.942	5.163	2.671	1.358	0.668	0.293	0.133	0.074	0.038
		σ	±7.04	±3.84	±2.11	±1.22	±0.63	±0.36	±0.21	±0.07	±0.03	±0.02
		% Var	36.36	35.99	19.40	4.533	1.400	0.655	0.362	0.110	0.038	0.007
TDR	IF	μ	20.35	9.867	4.806	2.334	0.966	0.289	0.131	0.073	0.041	0.017
		σ	±7.38	±4.32	±2.35	±1.27	±0.87	±0.29	±0.18	±0.08	±0.04	±0.02
		% Var	16.47	17.76	14.36	18.94	11.32	14.21	4.684	0.700	0.171	0.056
MRT	IF	μ	18.22	9.203	4.666	2.358	1.081	0.436	0.212	0.112	0.061	0.026
		σ	±6.12	±3.64	±2.04	±1.17	±0.68	±0.31	±0.12	±0.07	±0.03	±0.02
		% Var	25.88	24.01	16.52	13.73	8.328	9.395	1.538	0.295	0.056	0.019

HDR	IF	μ	19.84	9.646	4.729	2.357	1.124	0.398	0.175	0.098	0.050	0.025
		σ	±7.34	±4.25	±2.17	±1.16	±0.68	±0.41	±0.15	±0.06	±0.03	±0.02
		% Var	28.47	30.85	15.83	9.563	6.696	4.296	2.824	0.393	0.103	0.041
RPG	IF	μ	20.71	10.29	5.125	2.586	1.310	0.651	0.278	0.134	0.072	0.038
		σ	±7.14	±4.20	±2.29	±1.31	±0.76	±0.36	±0.21	±0.08	±0.04	±0.06
		% Var	23.76	33.56	22.73	9.678	4.705	1.205	0.743	0.223	0.033	0.013
CDG	IF	μ	20.38	10.08	4.979	2.335	1.025	0.379	0.178	0.095	0.051	0.027
		σ	±6.80	±3.98	±2.25	±1.30	±0.80	±0.32	±0.12	±0.06	±0.03	±0.02
		% Var	6.676	9.831	17.84	27.91	18.41	11.72	5.002	0.979	0.229	0.273
HSR	IF	μ	20.00	9.811	4.938	2.454	1.176	0.548	0.256	0.124	0.069	0.035
		σ	±7.06	±4.05	±2.25	±1.20	±0.73	±0.34	±0.17	±0.08	±0.04	±0.05
		% Var	28.83	20.21	25.46	10.46	13.44	1.630	0.803	0.244	0.066	0.019
BAG	IF	μ	6.426	2.845	1.253	0.762	0.259	0.159	0.062	0.031	0.017	0.003
		σ	±5.93	±2.62	±1.11	±0.71	±0.38	±0.27	±0.04	±0.02	±0.02	±0.01
		% Var	30.68	34.34	21.09	7.768	5.160	2.645	0.829	0.234	0.045	0.073
HAR	IF	μ	7.851	2.848	1.215	0.576	0.279	0.145	0.077	0.041	0.021	0.011
		σ	±7.11	±2.03	±0.76	±0.33	±0.15	±0.10	±0.04	±0.06	±0.04	±0.32
		% Var	7.389	21.83	27.76	25.53	12.42	5.613	1.087	0.291	0.036	0.058
JAU	IF	μ	7.990	3.371	1.606	0.774	0.369	0.215	0.113	0.058	0.027	0.009
		σ	±6.63	±2.31	±1.13	±0.51	±0.24	±0.38	±0.08	±0.06	±0.01	±0.004
		% Var	20.88	27.03	25.32	17.92	5.133	1.632	0.359	0.105	0.031	0.037
KSN	IF	μ	14.59	3.487	1.567	0.669	0.253	0.107	0.056	0.031	0.015	0.010
		σ	±11.5	±3.59	±1.22	±0.56	±0.23	±0.10	±0.04	±0.04	±0.04	±0.06
		% Var	10.08	9.004	12.53	18.87	13.70	19.98	2.349	0.307	0.030	0.031
LAK	IF	μ	5.829	2.656	1.282	0.610	0.300	0.146	0.076	0.038	0.025	0.014
		σ	±6.03	±1.69	±0.66	±0.30	±0.18	±0.09	±0.04	±0.04	±0.12	±0.03
		% Var	33.73	18.04	18.08	11.62	8.982	4.533	0.637	0.113	0.061	0.083
LEH	IF	μ	7.345	2.953	1.370	0.658	0.331	0.165	0.086	0.047	0.029	0.015
		σ	±6.54	±1.95	±0.79	±0.34	±0.24	±0.12	±0.04	±0.03	±0.22	±0.23
		% Var	16.13	30.27	22.75	12.75	7.288	2.032	0.887	0.197	0.008	0.013
MAH	IF	μ	11.26	3.167	1.557	0.716	0.323	0.158	0.071	0.044	0.023	0.014
		σ	±9.91	±2.36	±1.11	±0.64	±0.21	±0.35	±0.06	±0.03	±0.04	±0.02
		% Var	15.62	28.03	20.59	13.08	7.104	6.375	1.819	0.284	0.214	0.013
MTR	IF	μ	8.262	3.015	1.500	0.646	0.258	0.124	0.078	0.039	0.019	0.011
		σ	±7.62	±2.34	±1.24	±0.45	±0.21	±0.07	±0.09	±0.10	±0.16	±0.04
		% Var	7.804	21.29	26.96	18.31	10.27	10.28	1.537	0.133	0.039	0.013
PTN	IF	μ	8.820	3.439	1.336	0.792	0.405	0.215	0.092	0.048	0.018	0.009
		σ	±7.99	±3.36	±1.05	±0.79	±0.45	±0.21	±0.15	±0.17	±0.03	±0.02
		% Var	22.67	31.42	24.55	13.15	2.467	1.681	0.249	0.091	0.014	0.016
UTR	IF	μ	5.134	2.150	1.030	0.500	0.248	0.128	0.070	0.036	0.010	0.007
		σ	±3.71	±1.22	±0.51	±0.23	±0.12	±0.07	±0.05	±0.02	±0.02	±0.01
		% Var	19.71	38.59	20.95	12.17	5.921	0.873	0.161	0.047	0.083	0.034

KTP	IF	μ	11.56	4.338	2.023	1.110	0.562	0.235	0.151	0.073	0.044	0.019
		σ	±8.54	3.28	1.44	0.85	0.56	0.17	0.18	0.05	0.03	0.02
		% Var	37.91	31.75	16.99	5.215	1.365	2.478	0.329	0.037	0.012	0.015
PTN	IF	μ	9.353	4.844	2.066	1.041	0.387	0.217	0.093	0.052	0.020	0.013
		σ	±6.60	±3.71	±1.34	±0.99	±0.31	±0.23	±0.06	±0.06	±0.01	±0.06
		% Var	9.515	14.57	11.99	19.51	30.81	6.901	0.689	0.730	0.626	0.440
THM	IF	μ	17.71	5.896	2.328	1.064	0.291	0.189	0.061	0.036	0.020	0.012
		σ	±9.87	±4.40	±2.35	±1.46	±0.76	±0.11	±0.12	±0.03	±0.01	±0.02
		% Var	0.336	4.102	13.48	12.13	49.46	7.612	1.116	0.219	0.145	0.111
TVU	IF	μ	10.06	3.029	1.151	0.607	0.275	0.133	0.066	0.051	0.031	0.014
		σ	±9.50	±2.31	±1.11	±0.69	±0.47	±0.38	±0.10	±0.04	±0.05	±0.10
		% Var	3.450	16.23	30.50	21.45	23.44	1.222	0.236	0.023	0.009	0.008
KATNP	IF	μ	38.11	10.38	4.506	2.125	0.846	0.300	0.194	0.117	0.050	0.026
		σ	±30.3	±9.17	±3.36	±1.43	±0.80	±0.20	±0.14	±0.15	±0.04	±0.04
		% Var	1.106	3.661	4.668	4.271	27.74	54.08	2.562	0.188	0.071	0.075

888

889 **Table 7.** Regression Coefficients of the GMPE for all the 21 GMPs.

SL. NO.	GMP	Comp	c_0	c_1	c_2	c_3	c_4	c_5	c_6	c_7	σ_{inter}	σ_{intra}	σ
1	PGA	H	-2.733	0.640	-0.0029	-0.909	3.23E+06	-1.392	-0.028	0.106	0.184	0.427	0.465
		V	-5.951	0.867	-0.0020	-0.857	3.73E+06	-1.687	-0.047	0.071	0.159	0.431	0.459
2	PGV	H	5.577	0.664	-0.0024	-1.497	3.67E+06	-1.400	-0.089	0.262	0.338	0.483	0.589
		V	3.857	0.788	-0.0018	-1.502	2.95E+06	-1.405	-0.123	0.094	0.399	0.446	0.598
3	PGD	H	4.405	0.923	-0.0016	-1.729	2.90E+06	-1.386	-0.225	0.433	0.421	0.505	0.657
		V	-2.492	1.475	-0.0013	-1.362	1.45E+06	-1.386	-0.220	0.115	0.268	0.694	0.744
4	V/H		4.442	-0.875	-0.0002	0.277	4.45E+05	-1.402	0.203	-0.282	0.356	0.810	0.885
5	F_p	H	4.657	-0.967	0.0001	0.386	9.53E+04	-1.190	0.082	-0.151	0.503	1.049	1.163
		V	4.254	-0.538	0.0012	0.103	4.51E+06	-2.628	0.045	-0.207	0.194	0.333	0.385
6	Ω	H	5.105	-0.388	0.0014	-0.159	1.17E+06	-1.885	0.039	-0.099	0.146	0.264	0.302
		V	-0.783	0.093	0.0003	-0.069	1.14E+04	-1.038	-0.018	0.042	0.068	0.155	0.169
7	Q	H	-12.126	0.862	-0.0005	0.733	2.85E+06	-1.015	-0.005	0.004	0.130	0.162	0.208
		V	-3.236	0.409	0.0002	-0.296	1.71E+05	-1.511	-0.063	0.200	0.122	0.404	0.422
8	V/A	H	-5.202	0.580	-0.0002	-0.115	4.17E+05	-3.690	-0.095	0.093	0.217	0.537	0.579
		V	8.128	-0.660	0.0018	0.136	7.24E+05	-1.797	0.066	0.122	0.341	0.404	0.528
9	T_{sig}	H	7.131	-0.591	0.0015	0.291	2.12E+05	-1.557	0.102	0.077	0.248	0.445	0.510
		V	0.970	-0.104	0.0007	-0.187	6.75E+05	-1.748	-0.009	-0.044	0.074	0.338	0.346
10	a_{RMS}	H	-12.379	1.453	-0.0028	-0.630	4.09E+06	-2.028	-0.097	0.100	0.327	0.511	0.607
		V	15.956	-0.329	-0.0012	-3.093	1.78E+05	-0.845	-0.054	0.104	0.259	0.515	0.576
11	I_a	H	109.891	-0.984	0.0033	-14.714	8.57E+03	-0.315	-0.102	0.298	0.331	0.785	0.852
		V	39.312	-0.819	-0.0010	-5.305	1.78E+05	-0.842	-0.013	0.287	0.408	0.743	0.848
12	CAV	H	10.004	0.204	-0.0006	-1.049	2.90E+06	-1.386	-0.042	0.242	0.261	0.408	0.484
		V	18.599	-0.519	-0.0002	-1.624	1.82E+06	-1.205	0.028	0.216	0.317	0.353	0.474
13	I_c	H	-0.955	1.494	-0.0035	-0.964	4.02E+07	-2.026	-0.113	0.224	0.343	0.642	0.728
		V	10.418	0.507	-0.0022	-1.871	2.67E+06	-1.399	-0.047	0.212	0.372	0.614	0.718
14	ASI	H	0.968	0.838	-0.0030	-0.643	7.14E+06	-1.579	-0.013	0.102	0.188	0.415	0.456
		V	-0.221	1.086	-0.0018	-0.949	1.50E+04	-0.849	-0.013	0.058	0.200	0.397	0.445
15	VSI	H	1.566	0.984	-0.0027	-1.036	5.18E+06	-1.529	-0.077	0.341	0.325	0.555	0.644
		V	3.344	1.023	-0.0020	-1.438	2.19E+05	-1.013	-0.161	0.148	0.384	0.482	0.616
16	E_{acc}	H	17.227	0.217	-0.0041	-2.654	3.40E+06	-1.281	-0.113	0.323	0.391	0.815	0.904
		V	64.559	-0.847	0.0025	-9.115	1.75E+04	-0.492	-0.021	0.271	0.312	0.719	0.783
17	E_w	H	3.889	-0.597	0.0006	0.221	1.75E+05	-3.366	0.036	-0.219	0.228	0.400	0.461
		V	5.805	-0.534	0.0013	-0.158	1.05E+06	-1.434	0.070	-0.117	0.194	0.309	0.365
18	S_w	H	3.665	-0.441	0.0014	0.008	6.78E+06	-2.216	0.001	-0.144	0.129	0.387	0.408
		V	3.488	-0.208	0.0012	-0.164	1.20E+05	-1.451	0.047	-0.091	0.015	0.304	0.304
19	E_t	H	4.078	-0.205	0.0005	0.440	3.37E+06	-3.109	0.028	-0.019	0.172	0.293	0.340
		V	4.182	-0.253	0.0006	0.465	3.76E+05	-1.669	0.045	-0.030	0.173	0.343	0.384
20	S_t	H	5.042	-0.483	0.0009	0.392	3.45E+05	-1.646	0.072	0.009	0.265	0.318	0.414
		V	4.276	-0.435	0.0006	0.520	2.13E+05	-1.549	0.086	-0.005	0.196	0.356	0.406
21	ρ*	H	1.179	-0.160	0.0005	-0.036	-5.64E-03	-2.500	0.044	-0.069	0.050	0.172	0.179
		V	0.625	-0.085	0.0003	-0.007	-7.50E-05	0.893	0.025	-0.048	0.027	0.174	0.176

890 *The coefficients of ρ are derived for non-logarithmic values

891 **Table 8.** Rankings and normalized average rankings obtained for the GMPEs of PGA

Rank	GMPE	EDR	EDR_N	GMPE	LH	LH_N	GMPE	LLH	LLH_N
1	This study	0.575	1.000	This study	0.536	1.071	BSSA14	1.701	1.000
2	SSSA17	0.806	1.402	CY14	0.526	1.051	ASK14	1.787	1.051
3	CB14	1.596	2.777	K06	0.435	0.870	This study	1.792	1.053
4	K06	1.754	3.052	ASK14	0.411	0.823	SSSA17	1.820	1.070
5	ASK14	1.783	3.102	BSSA14	0.409	0.817	CB14	1.879	1.105
6	CY14	1.883	3.276	SSSA17	0.377	0.755	CY14	1.895	1.114
7	BSSA14	1.968	3.424	CB14	0.325	0.650	Z06	2.348	1.381
8	Z06	2.563	4.461	Z06	0.109	0.218	K06	2.582	1.518

892

893 **Table 9.** Rankings and normalized average rankings obtained for the GMPEs of PGV

Rank	GMPE	EDR	EDR_N	GMPE	LH	LH_N	GMPE	LLH	LLH_N
1	This study	0.811	1.000	This study	0.536	1.071	K06	1.564	1.000
2	K06	0.969	1.195	CY14	0.508	1.016	This study	1.611	1.030
3	SSSA17	1.089	1.344	SSSA17	0.493	0.986	SSSA17	1.686	1.078
4	CB14	1.754	2.163	K06	0.440	0.879	CY14	1.885	1.205
5	CY14	1.834	2.263	ASK14	0.324	0.647	CB14	1.933	1.236
6	ASK14	1.856	2.289	BSSA14	0.312	0.625	ASK14	1.939	1.239
7	BSSA14	2.118	2.613	CB14	0.246	0.492	BSSA14	1.965	1.256

894

895 **Table 10.** Rankings and normalized average rankings obtained for the GMPEs of PGD

Rank	GMPE	EDR	EDR_N	GMPE	LH	LH_N	GMPE	LLH	LLH_N
1	This study	1.069	1.000	This study	0.517	1.035	This study	1.373	1.000
2	SSSA17	1.393	1.303	SSSA17	0.393	0.786	SSSA17	1.519	1.106
3	CB08	2.183	2.042	CB08	0.129	0.259	CB08	2.127	1.549

896

897 **Table 11.** Rankings and normalized average rankings obtained for the GMPEs of I_a

Rank	GMPE	EDR	EDR_N	GMPE	LH	LH_N	GMPE	LLH	LLH_N
1	This study	1.056	1.000	This study	0.588	1.176	FPG14	1.532	1.000
2	FPG14	2.180	2.063	FPG14	0.530	1.059	This study	1.583	1.034
3	SS98	3.466	3.281	SS98	0.215	0.431	SS98	2.076	1.355
4	A09	5.838	5.526	A09	0.004	0.008	A09	3.496	2.282

898

899 **Table 12.** Rankings and normalized average rankings obtained for the GMPEs of CAV

Rank	GMPE	EDR	EDR_N	GMPE	LH	LH_N	GMPE	LLH	LLH_N
1	This study	0.595	1.000	CB10	0.622	1.243	CB10	1.570	1.000
2	CB10	0.706	1.186	This study	0.498	0.995	This study	1.650	1.051
3	DW13	0.864	1.453	DW13	0.376	0.753	FPG14	1.655	1.054
4	FPG14	1.125	1.892	FPG14	0.330	0.659	DW13	1.932	1.231

900

Table 13. Final rankings for the GMPEs of PGA, PGV and PGD with respect to logic-tree-based normalized ranking indices

PGA			PGV			PGD		
Rank	GMPE	RI_N	Rank	GMPE	RI_N	Rank	GMPE	RI_N
1	This study	1.031	1	This study	1.025	1	This study	1.009
2	SSSA17	1.157	2	K06	1.067	2	SSSA17	1.125
3	CB14	1.827	3	SSSA17	1.188	3	CB08	1.473
4	ASK14	2.019	4	CB14	1.514			
5	K06	2.123	5	ASK14	1.616			
6	BSSA14	2.166	6	CY14	1.687			
7	CY14	2.179	7	BSSA14	1.777			
8	Z06	2.630						

904 **Table 14.** Final rankings for the GMPEs of I_a and CAV with respect to logic-tree-based
905 normalized ranking indices

I_a			**CAV**		
Rank	GMPE	RI_N	Rank	GMPE	RI_N
1	This study	1.052	1	This study	1.012
2	FPG14	1.546	2	CB10	1.154
3	SS98	2.087	3	DW13	1.222
4	A09	3.335	4	FPG14	1.374

906

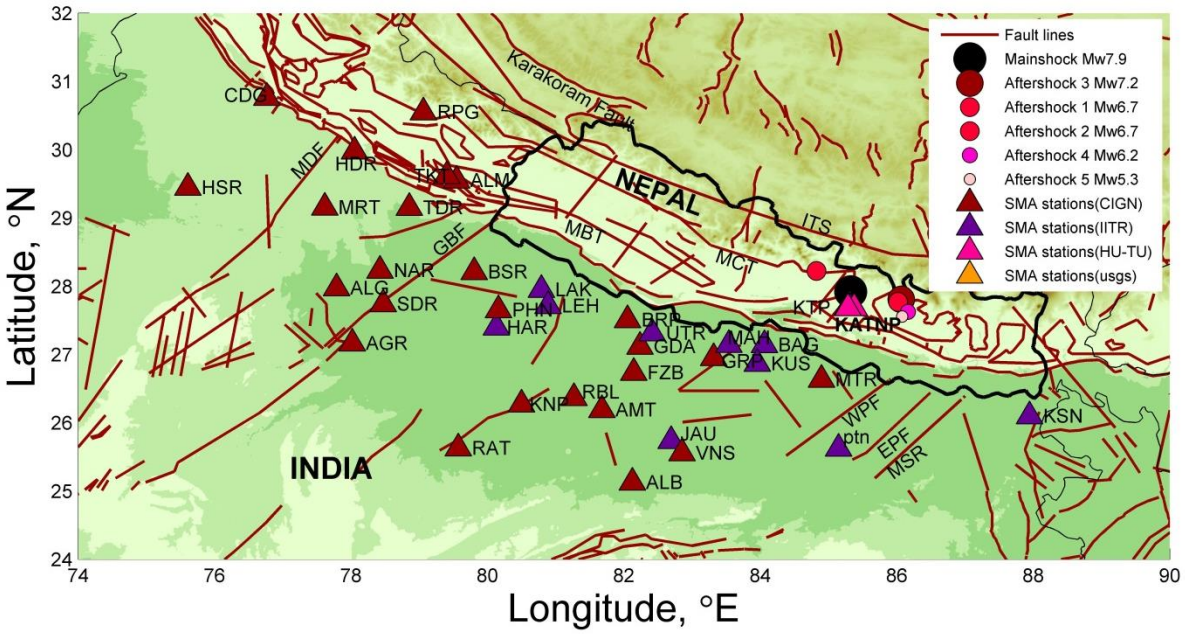

MBT	:	Main Boundary Thrust	ITS	:	Indus Tsangpo Suture
MCT	:	Main Central Thrust	MDF	:	Mahendragarh Dehradun Fault
WPF	:	West Patna Fault	GBF	:	Great Boundary Fault
EPF	:	East Patna Fault	MSR	:	MungherSaharsa Ridge

Fig. 1 Tectonic map of Nepal showing epicentres of all the six earthquakes and the corresponding ground motion recording stations considered in this study

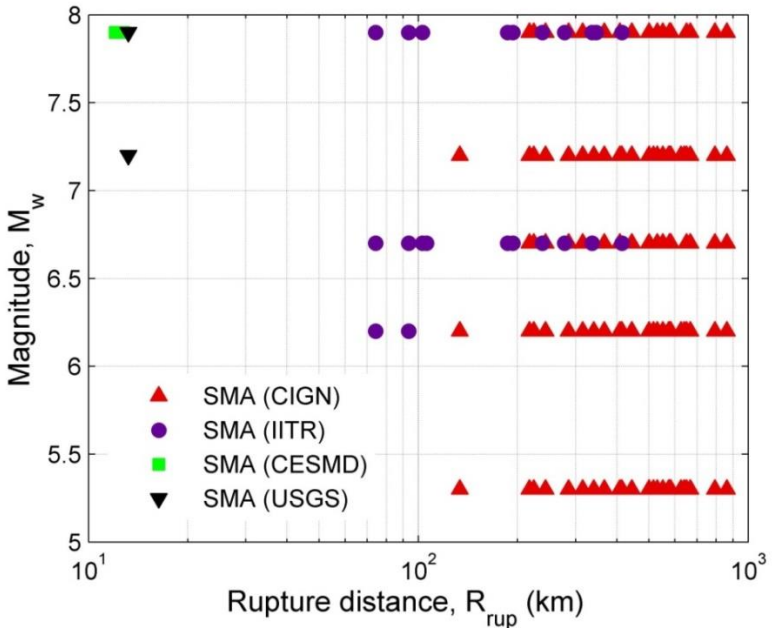

911

912 **Fig. 2** Distribution of ground motion records with respect to Moment magnitude (M_w) and
913 Rupture distance (R_{rup})

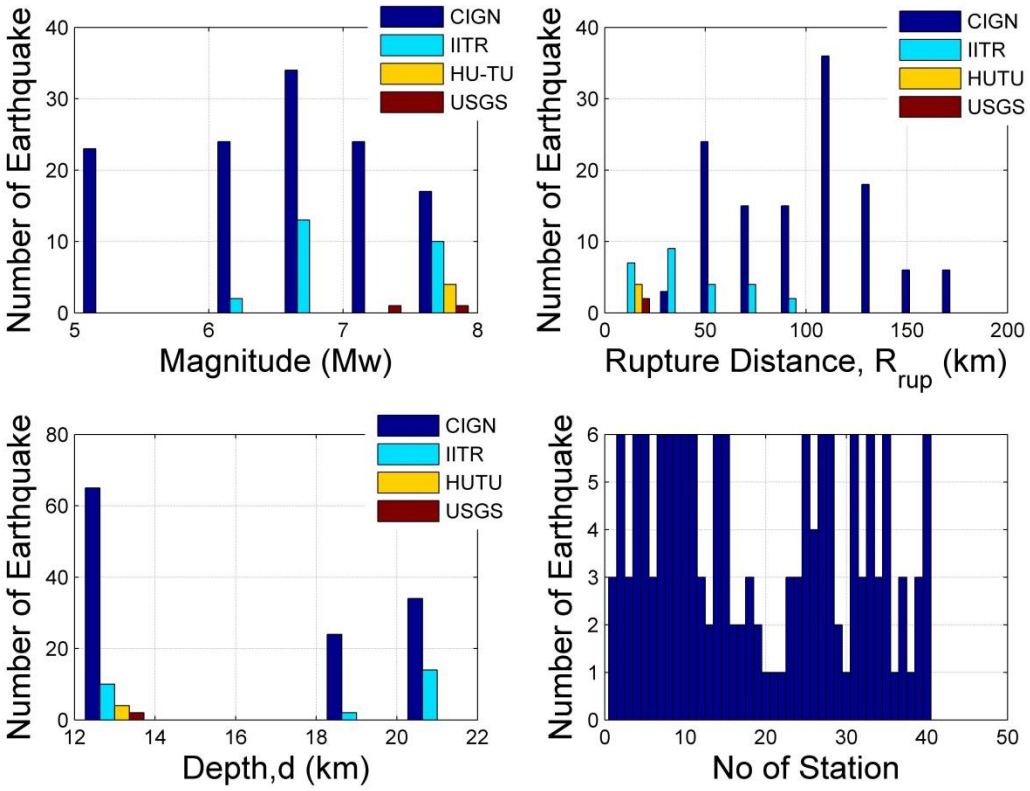

Fig. 3 Histograms showing the distribution of ground motion records used in the current study with respect to Moment magnitude (M_w), Rupture distance (R_{rup}) and Hypocentral depth (d)

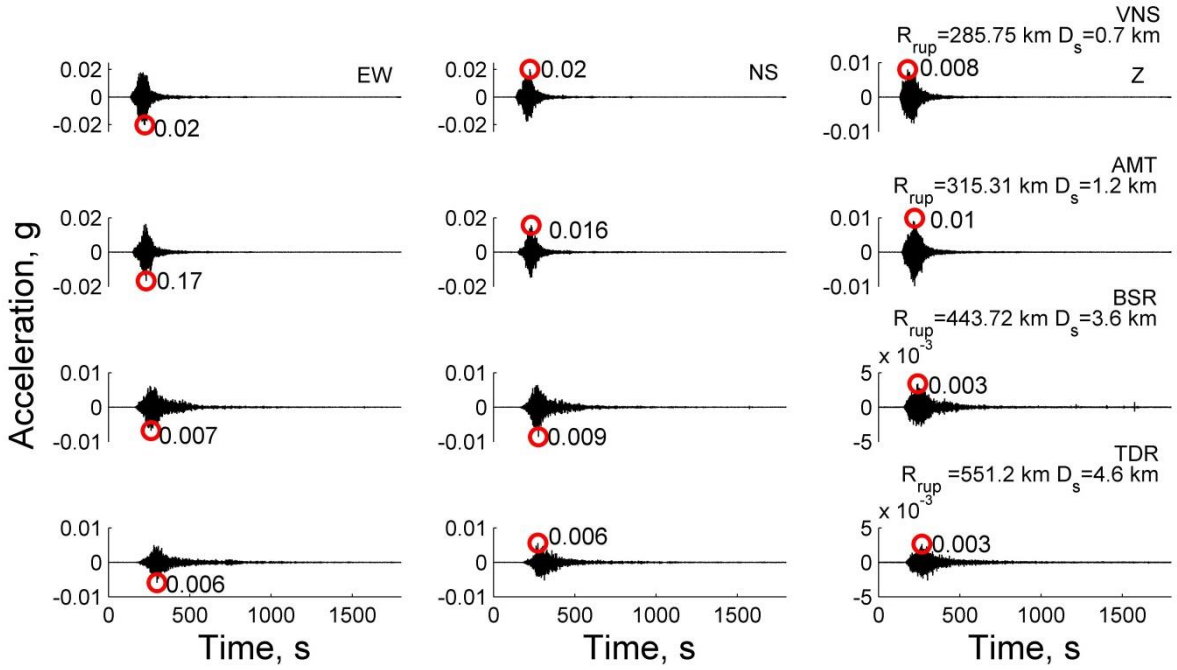

(a)

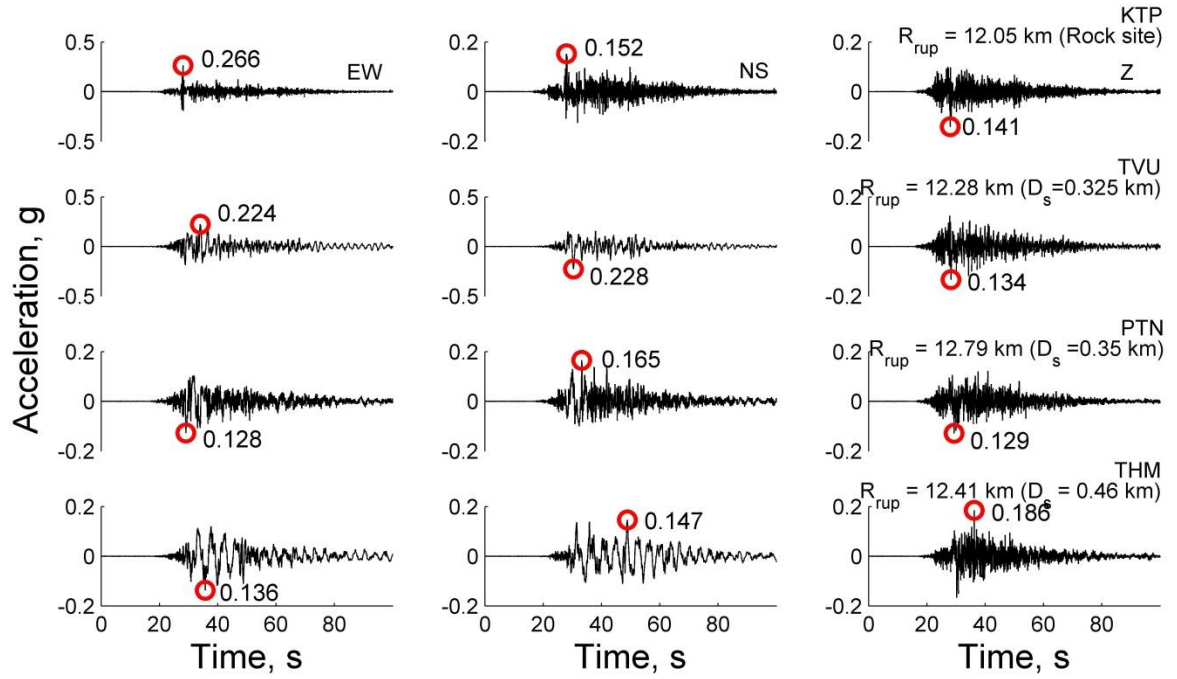

(b)

Fig. 4 Acceleration time histories (EW, NS and UD component) of the M_w 7.9 Nepal earthquake, recorded at stations: (a) VNS, AMT, BSR and TDR in the IG basin and (b) KTP, TVU, PTN and THM in the Kathmandu basin

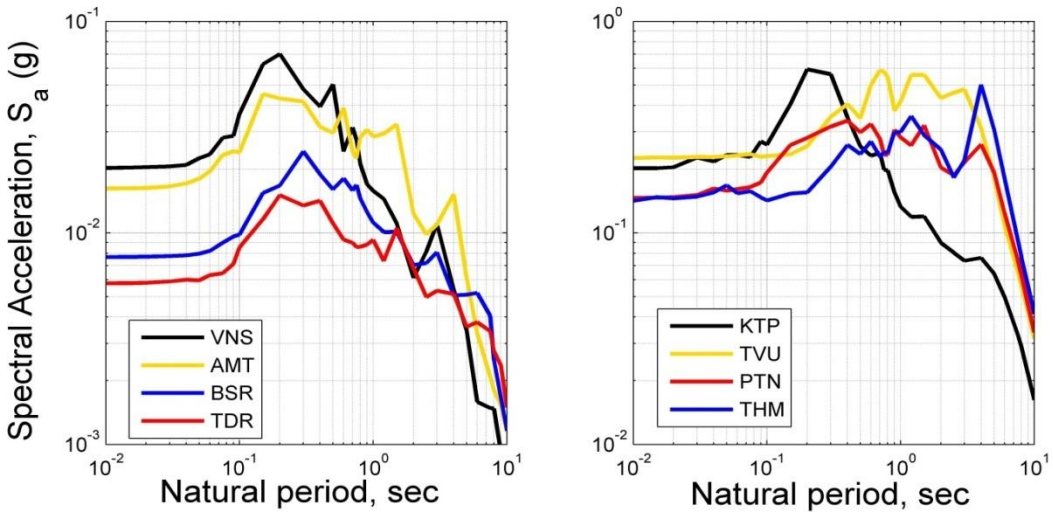

925

926 **Fig. 5** Acceleration response spectra obtained for the time histories (of Figure 4) of stations:
927 (a) VNS, AMT, BSR and TDR in the IG basin and (b) KTP, TVU, PTN and THM in the
928 Kathmandu basin

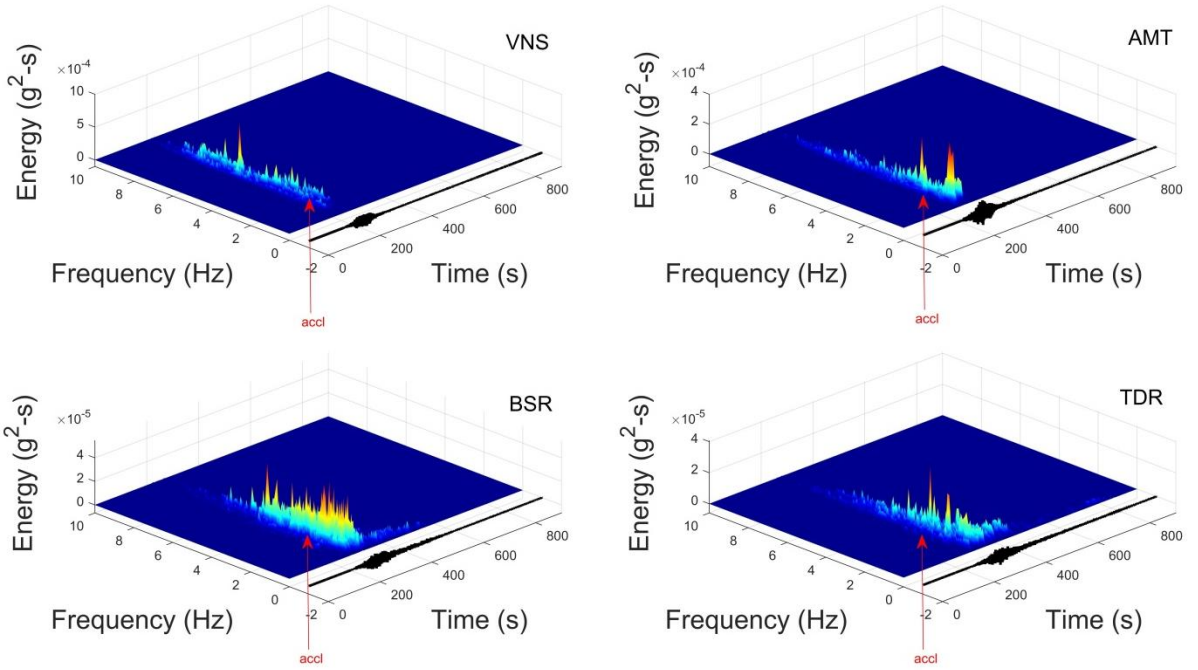

(a)

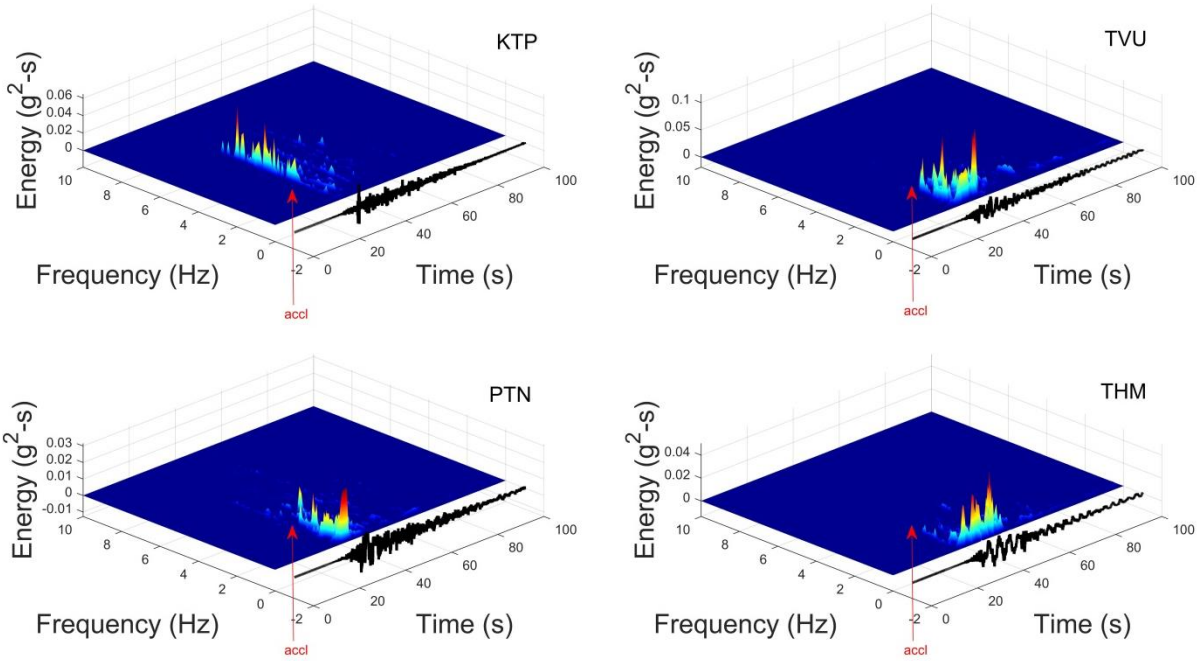

(b)

Fig. 6 Hilbert Energy Spectrum for acceleration time histories (EW component) of the M_w 7.9 Nepal earthquake, recorded at stations (a) VNS, AMT, BSR and TDR in the IG basin and (b) KTP, TVU, PTN and THM in the Kathmandu basin. Hilbert Energy Spectrum for acceleration time histories (NS and Vertical component) for stations in IG basin and Kathmandu basin are shown in electronic supplement (NS – Figure A5 and Vertical Figure A6)

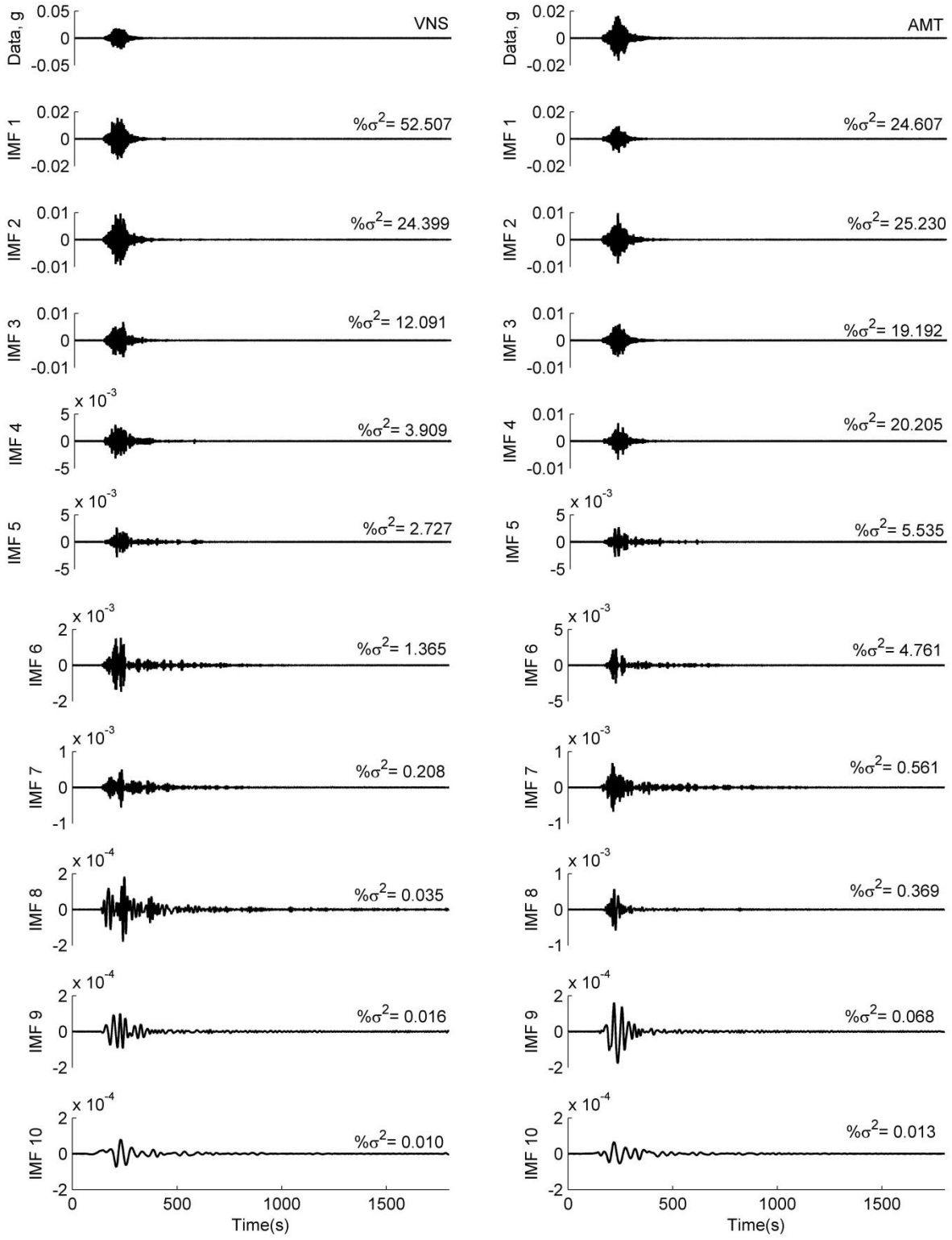

Fig. 7 Intrinsic mode functions (IMFs) for acceleration time histories (EW component) of the M_w 7.9 Nepal earthquake, recorded at stations: VNS, AMT, BSR and TDR in the IG basin and KTP, TVU, PTN and THM in the Kathmandu basin. Intrinsic mode functions (IMFs) for acceleration time histories (NS and Vertical component) recorded at the mentioned stations in IG basin and Kathmandu basin is shown in electronic supplement. (NS – Figure A1 and Vertical Figure A2)

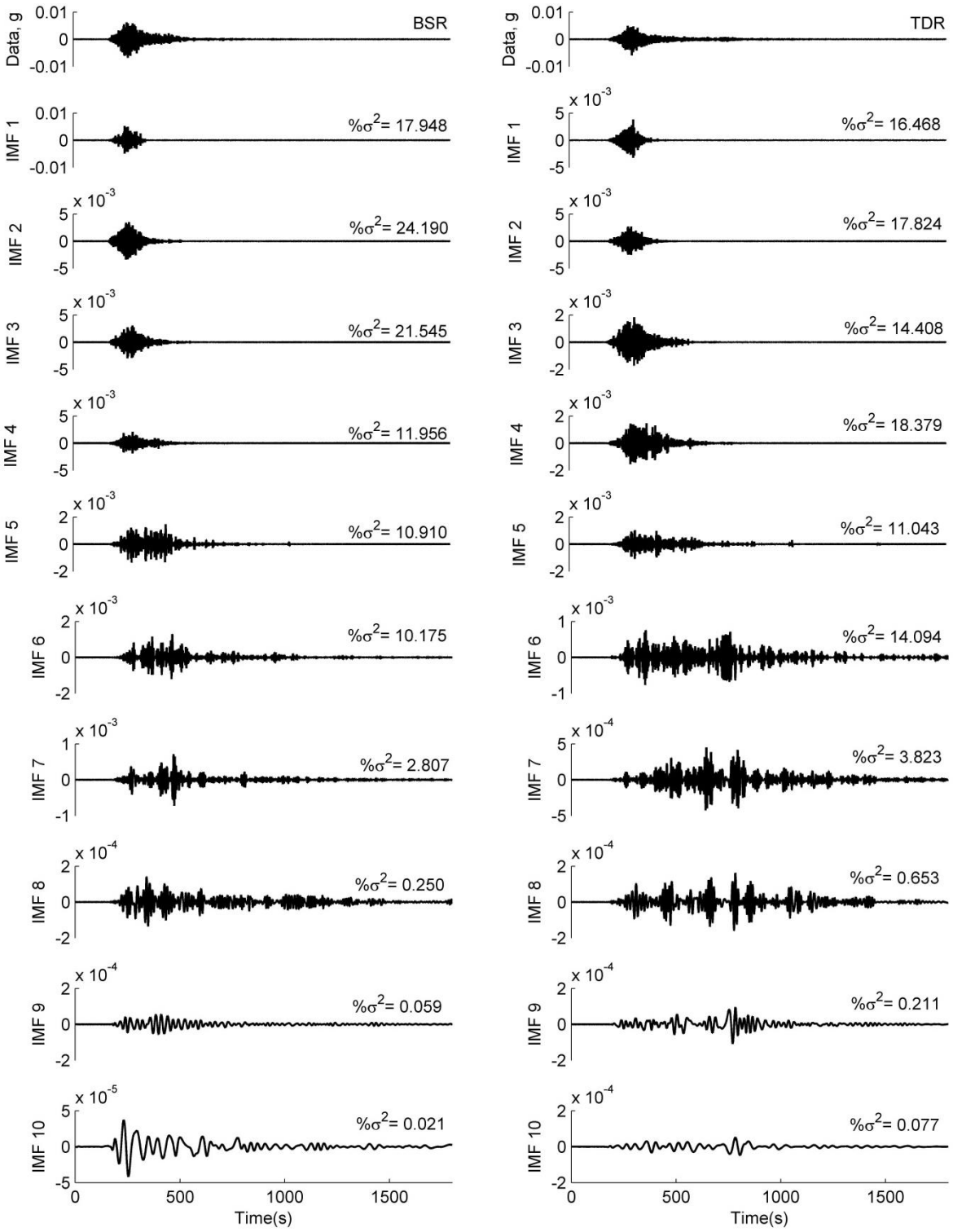

947

948

949 **Fig. 7** [Continued] Intrinsic mode functions (IMFs) for acceleration time histories of the Mw
950 7.9 Nepal earthquake, recorded at stations: VNS, AMT, BSR and TDR in the IG basin and
951 KTP, TVU, PTN and THM in the Kathmandu basin. Intrinsic mode functions (IMFs) for
952 acceleration time histories (NS and Vertical component) recorded at the mentioned stations in
953 IG basin and Kathmandu basin is shown in electronic supplement. (NS – Figure A1 and
954 Vertical Figure A2)

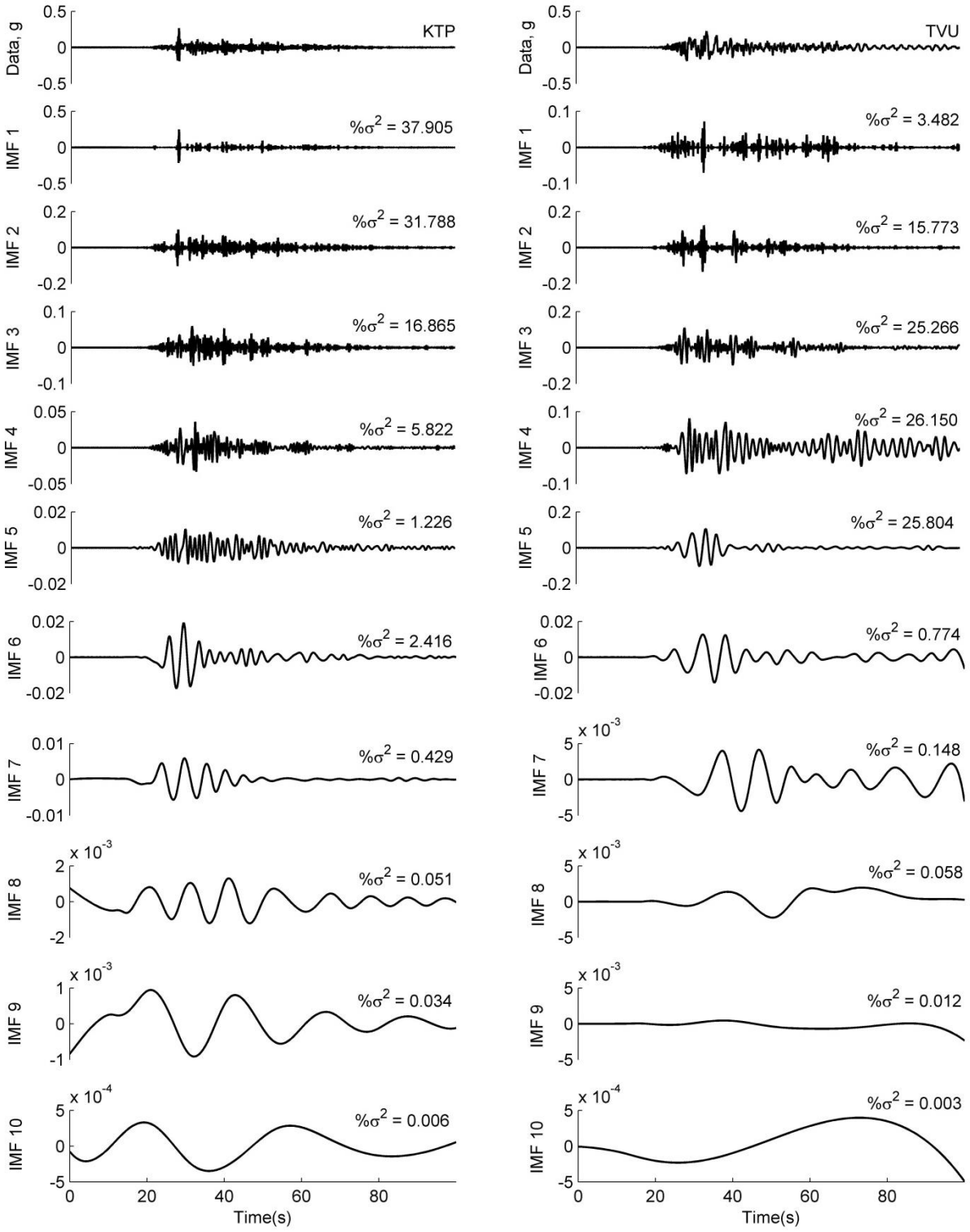

Fig. 7 [Continued] Intrinsic mode functions (IMFs) for acceleration time histories of the Mw 7.9 Nepal earthquake, recorded at stations: VNS, AMT, BSR and TDR in the IG basin and KTP, TVU, PTN and THM in the Kathmandu basin. Intrinsic mode functions (IMFs) for acceleration time histories (NS and Vertical component) recorded at the mentioned stations in IG basin and Kathmandu basin is shown in electronic supplement. (NS – Figure A1 and Vertical Figure A2)

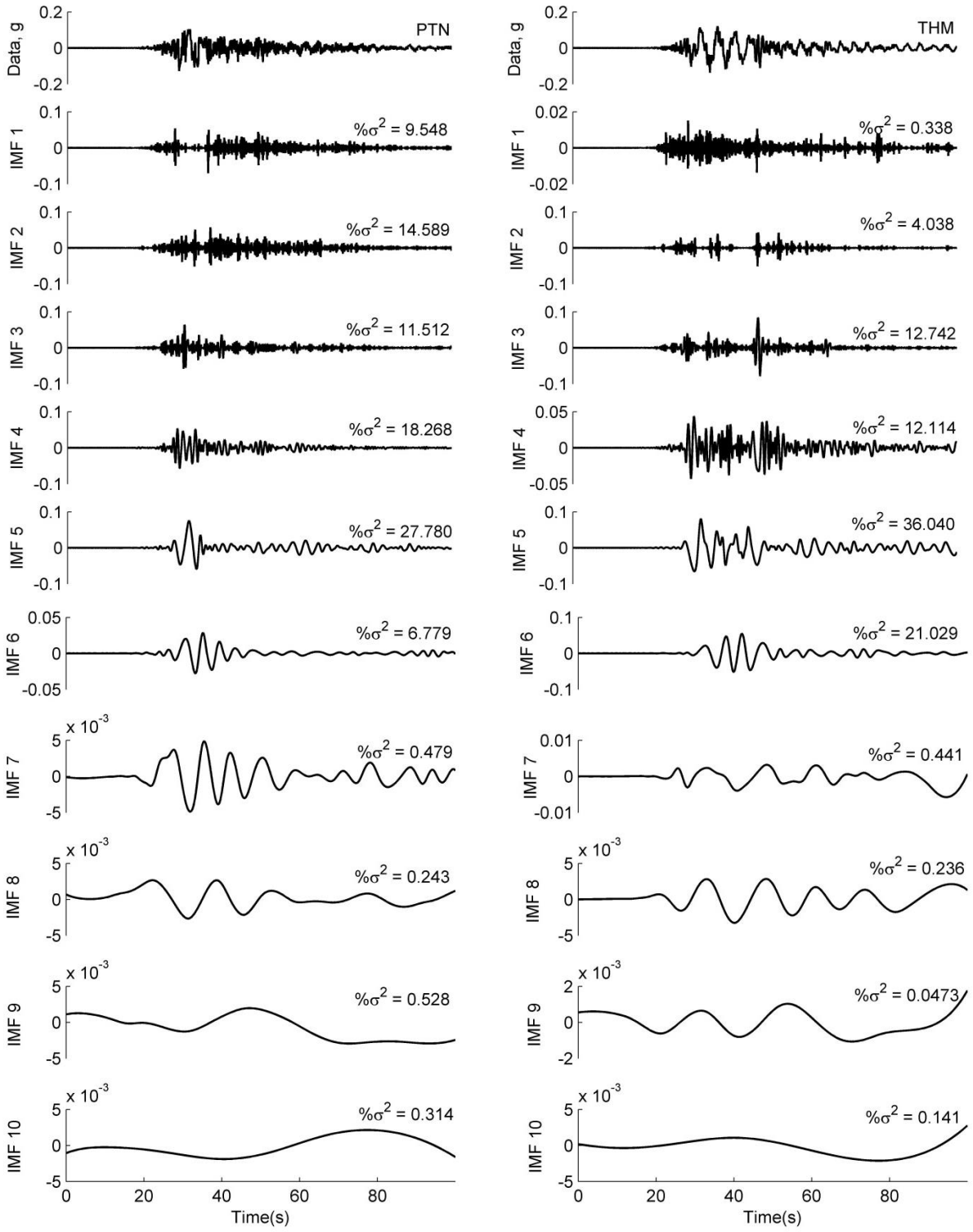

Fig. 7 [Continued] Intrinsic mode functions (IMFs) for acceleration time histories of the Mw 7.9 Nepal earthquake, recorded at stations: VNS, AMT, BSR and TDR in the IG basin and KTP, TVU, PTN and THM in the Kathmandu basin. Intrinsic mode functions (IMFs) for acceleration time histories (NS and Vertical component) recorded at the mentioned stations in IG basin and Kathmandu basin is shown in electronic supplement. (NS – Figure A1 and Vertical Figure A2)

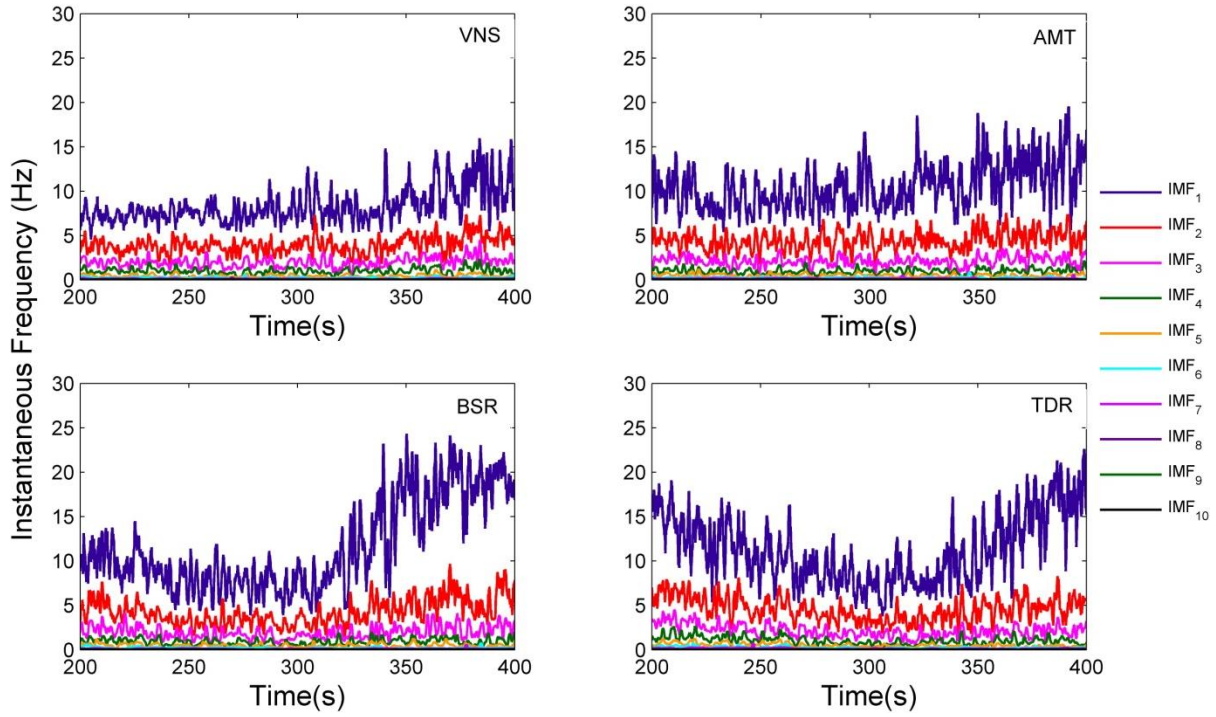

(a)

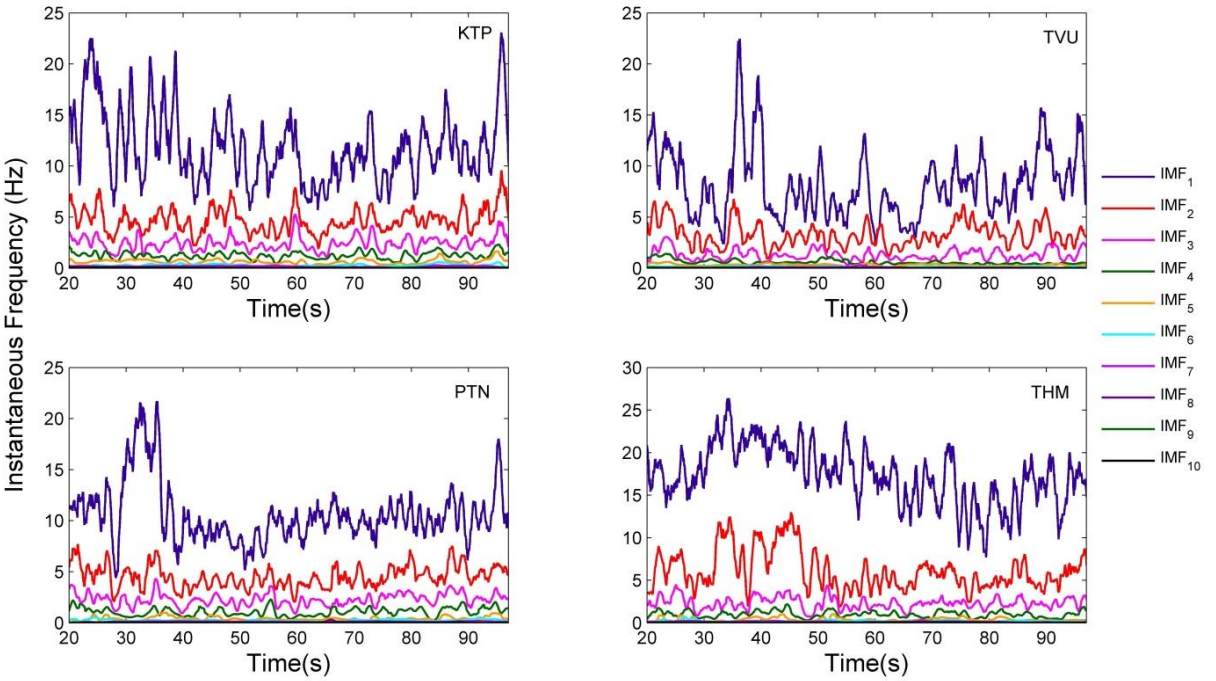

(b)

Fig. 8 Instantaneous frequencies of acceleration time histories (EW component) for stations (a) VNS, AMT, BSR and TDR in the IG basin and (b) KTP, TVU, PTN and THM in the Kathmandu basin. Instantaneous frequencies of acceleration time histories (NS and Vertical component) recorded at the mentioned stations in IG basin and Kathmandu basin is shown in electronic supplement. (NS – Figure A3 and Vertical Figure A4)

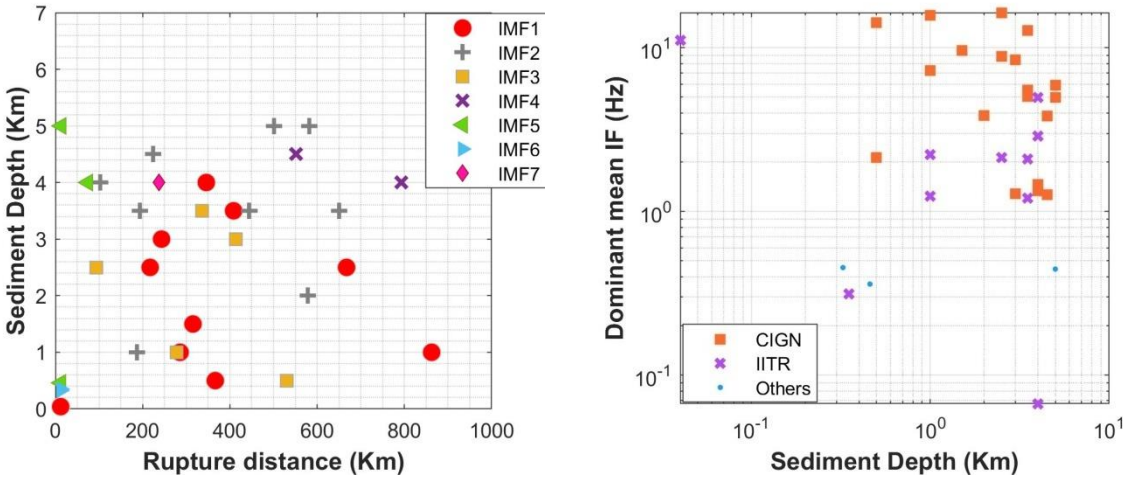

(a) (b)

Fig. 9 (a) Distribution of dominant Intrinstic Mode Functions (IMFs) of the ground motion time histories of the mainshock with rupture distance (Rrup) and Sediment depth (D); (b) Variation of dominant mean Instantaneous frequencies (Ifs) with respective site sediment depth values

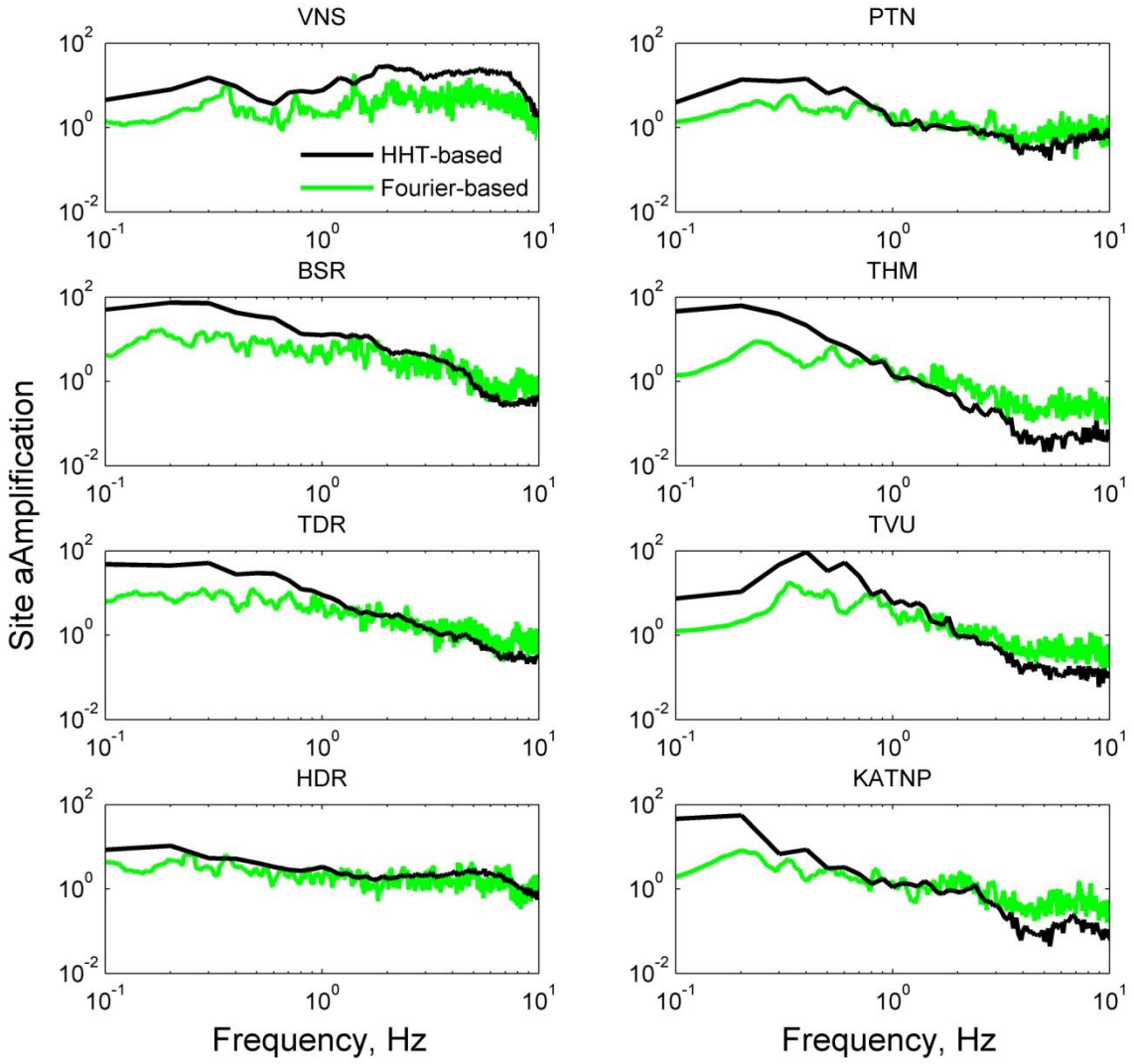

984

985 **Fig. 10** Comparison between HHT-based and Fourier based site amplifications for stations (a)
986 VNS, AMT, BSR and TDR with reference hard sites as ALB, ALM, ALM and RPG in the IG
987 basin and (b) TVU, PTN, THM and KATNP with KTP as reference hard site in the
988 Kathmandu basin

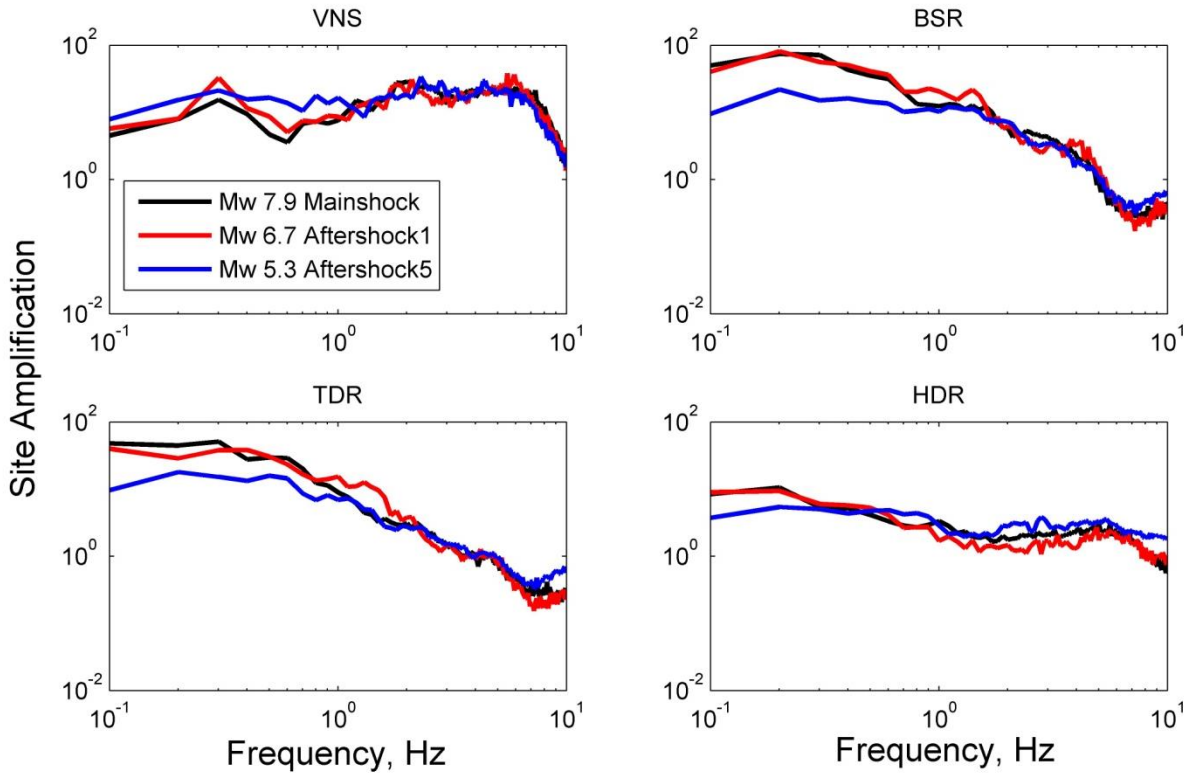

989

990 **Fig. 11** HHT-based site amplifications for stations VNS, AMT, BSR and TDR against the
991 reference sites ALB, ALM, ALM and RPG of the IG basin, for the M_w 7.9 mainshock and the
992 M_w 6.7 M_w 5.3) aftershocks

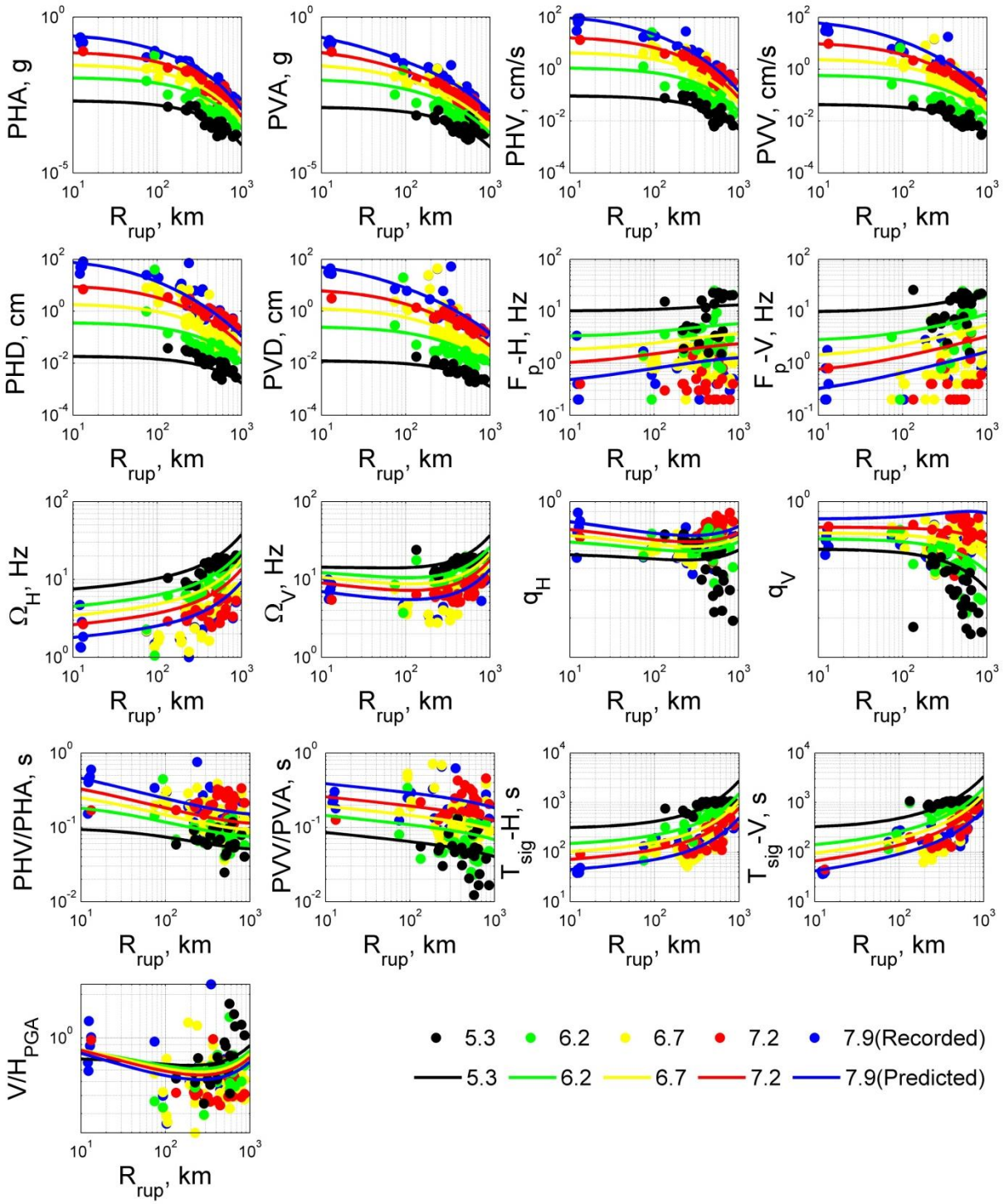
PHA, g
PVA, g
PHV, cm/s
PVV, cm/s
PHD, cm
PVD, cm
F_p-H, Hz
F_p-V, Hz
Ω_H, Hz
Ω_V, Hz
q_H
q_V
PHV/PHA, s
PVV/PVA, s
T_sig-H, s
T_sig-V, s
V/H_PGA
R_rup, km
5.3 6.2 6.7 7.2 7.9(Recorded)
5.3 6.2 6.7 7.2 7.9(Predicted)

(a)

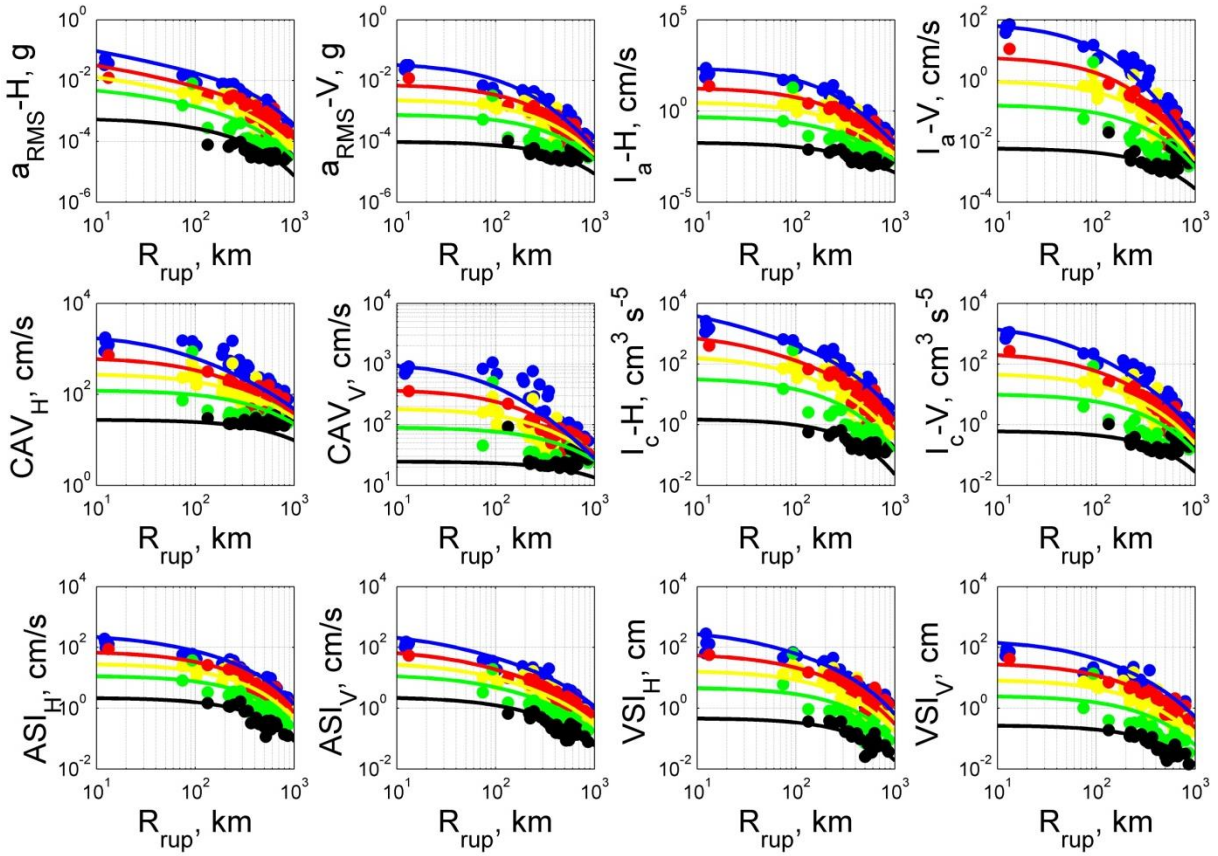
a_{RMS}-H, g
a_{RMS}-V, g
I_a-H, cm/s
I_a-V, cm/s
CAV_H, cm/s
CAV_V, cm/s
I_c-H, cm^3 s^{-5}
I_c-V, cm^3 s^{-5}
ASI_H, cm/s
ASI_V, cm/s
VSI_H, cm
VSI_V, cm
R_{rup}, km

(b)

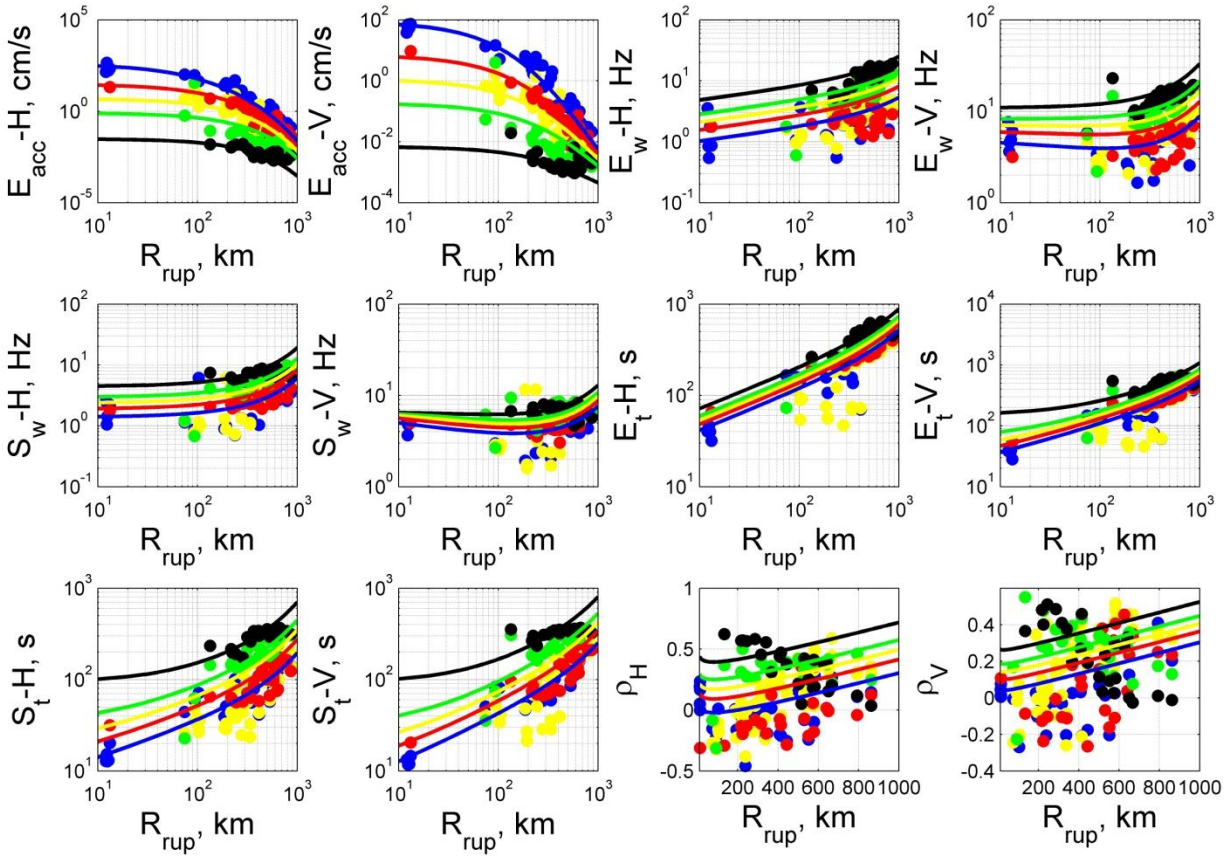
E_{acc}-H, cm/s
E_{acc}-V, cm/s
E_w-H, Hz
E_w-V, Hz
S_w-H, Hz
S_w-V, Hz
E_t-H, s
E_t-V, s
S_t-H, s
S_t-V, s
ρ_H
ρ_V
R_{rup}, km

(c)

Fig. 12 Variation of horizontal and vertical components of the 21 GMPs: (a) First order parameters, (b) Second order parameters and (c) Third order parameters, with rupture distance (R_{rup}), showing the recorded data (circular markers) and the predicted values (solid lines) for different moment magnitudes: M_w 7.9 – blue, M_w 7.2 - red, M_w 6.7 – yellow, M_w 6.2 -green, M_w 5.3 – black

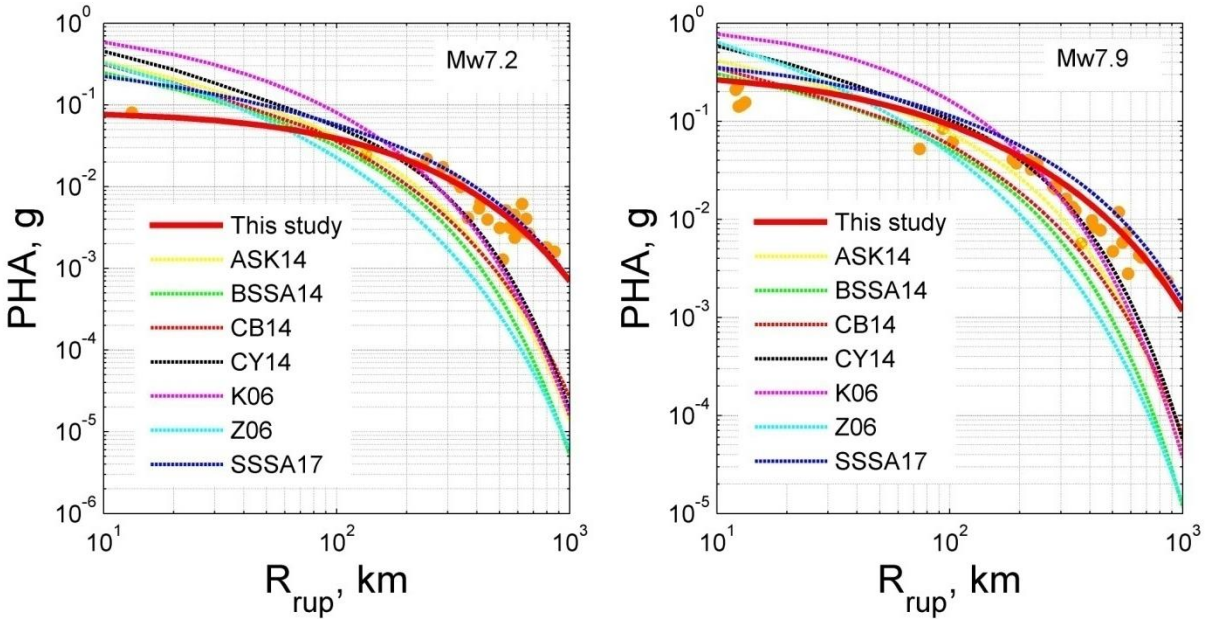

Fig. 13 Comparisons of the GMPE developed for PGA for IG basin with other empirical prediction equations: ASK14 – Abrahamson et al. (2014) BSSA14 – Boore et al. (2014); CB14 – Campbell and Bozorgnia (2014); CY14 – Chiou and Youngs (2014); K06 – Kanno et al. (2006), Z06 – Zhao et al. (2006) and SSSA17 – Singh et al. (2017)

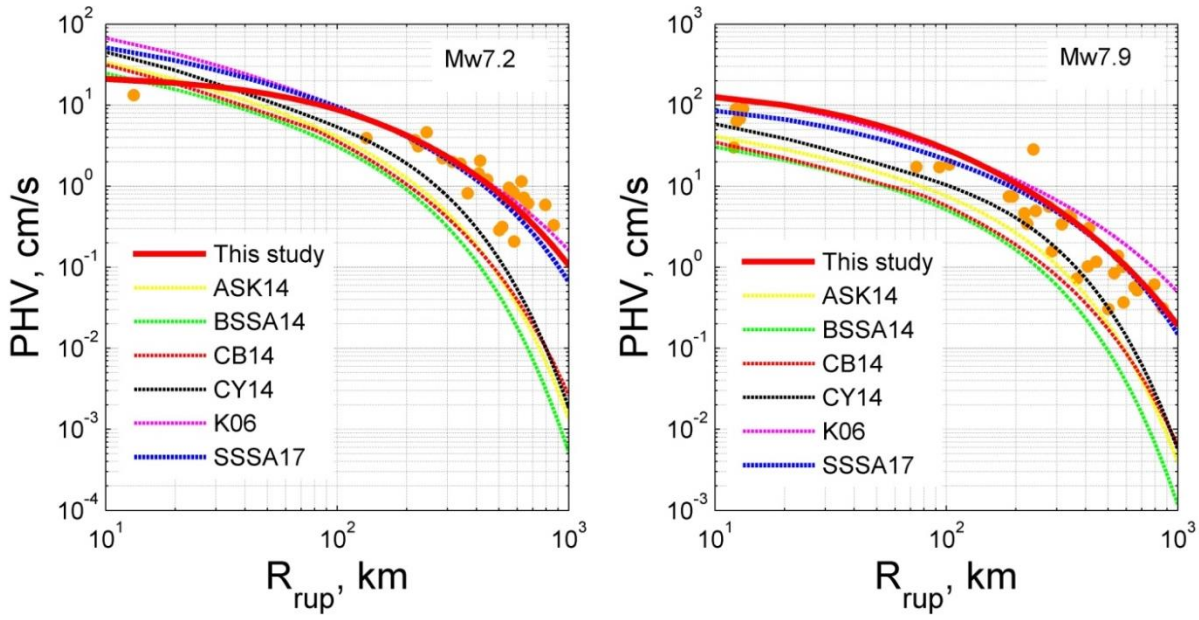

Fig. 14 Comparisons of the GMPE developed for PGV for IG basin with other empirical prediction equations: ASK14 – Abrahamson et al. (2014) BSSA14 – Boore et al. (2014); CB14 – Campbell and Bozorgnia (2014); CY14 – Chiou and Youngs (2014); K06 – Kanno et al. (2006) and SSSA17 – Singh et al. (2017)

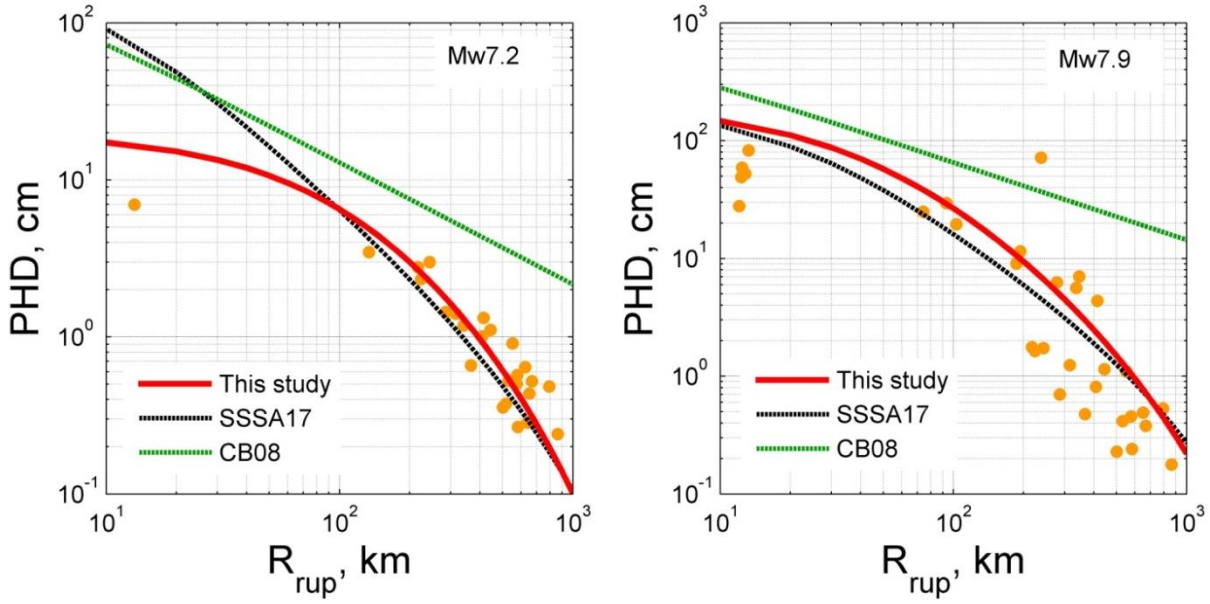

Fig. 15 Comparisons of the GMPE developed for PGD for IG basin with other empirical prediction equations: SSSA17 – Singh et al. (2017) and CB08 – Campbell and Bozorgnia (2008)

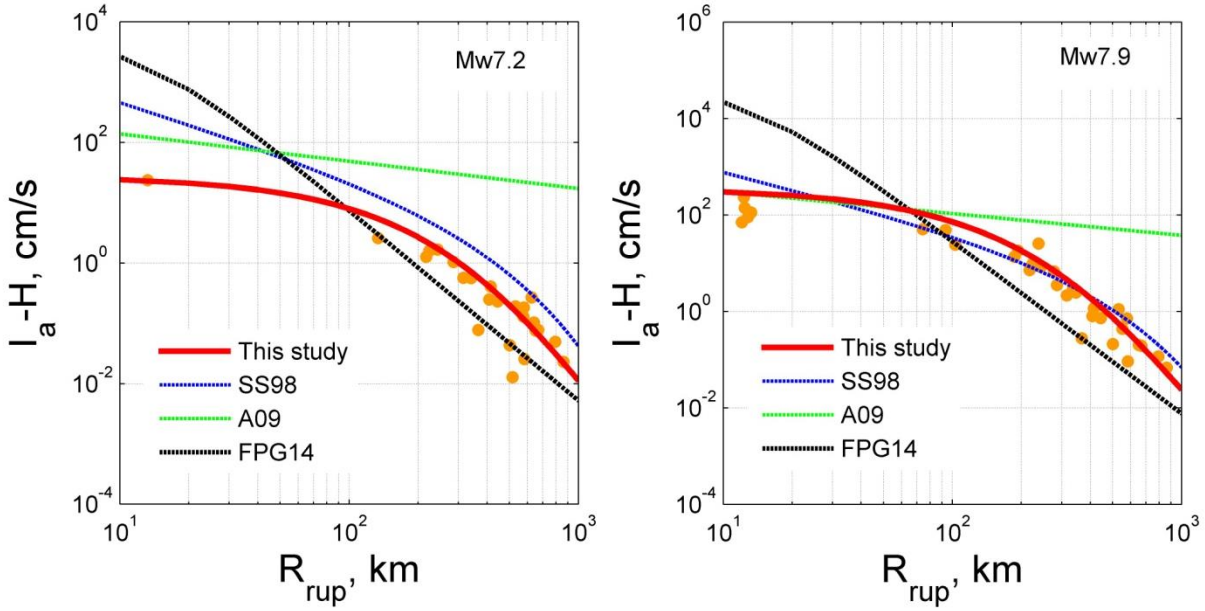

Fig. 16 Comparisons of the GMPE developed for Arias Intensity (I_a) for IG basin with other empirical prediction equations: SS98 – Sharma and Srbulov (1998), A09 – Amiri et al. (2009) and FPG14 – Foulser-Piggot and Goda (2014)

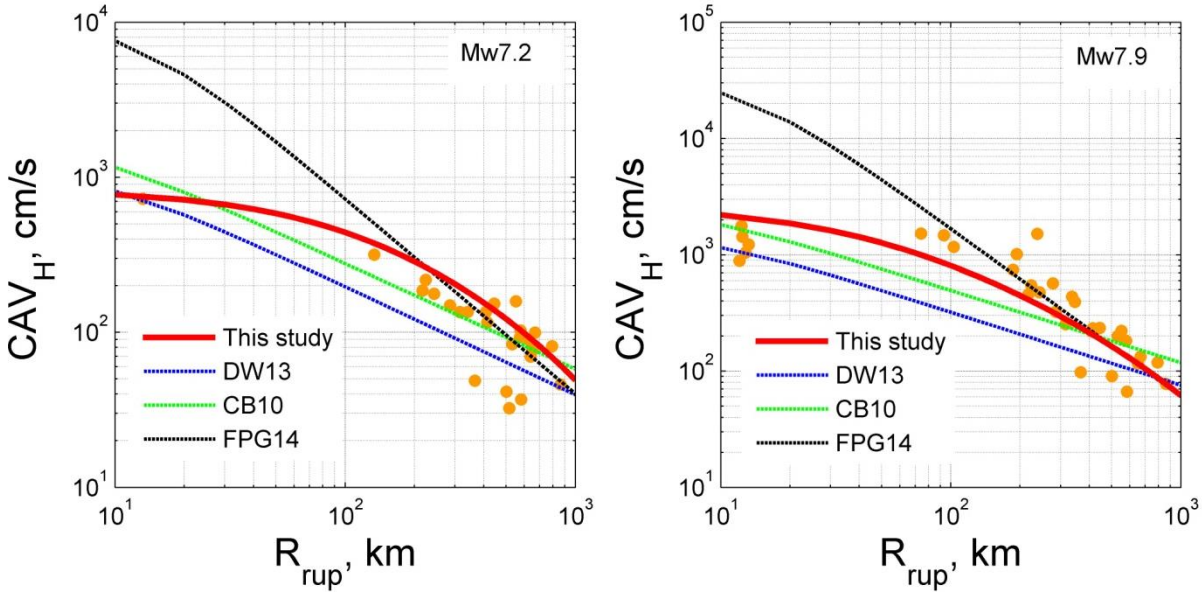

Fig. 17 Comparison of the GMPE developed in this study for CAV for IG basin with other empirical prediction equations: CB10 – Campbell and Bozorgnia (2010), FPG14 – Foulser-Piggot and Goda (2014) and DW13 – Du and Wang (2013)

Supplementary Files

This is a list of supplementary files associated with this preprint. Click to download.

- ElectronicSupplementGMPsfor2015NepalEarthquake.docx